FINITE ELEMENT ANALYSIS OF THE FORCED OSCILLATIONS OF SHIP HULL FORMS.

David Arthur Smith

NAVAL POSTGRADUATE SCHOOL
Monterey, California

THESIS

FINITE ELEMENT ANALYSIS OF THE FORCED OSCILLATION OF SHIP HULL FORMS

by

David Arthur Smith, Jr.

June 1974

Thesis Advisor: R.E. Newton

Approved for public release; distribution unlimited.

SECURITY CLASSIFICATION OF THIS PAGE *(When Data Entered)*

REPORT DOCUMENTATION PAGE

READ INSTRUCTIONS BEFORE COMPLETING FORM

1. REPORT NUMBER	2. GOVT ACCESSION NO. / 3. RECIPIENT'S CATALOG NUMBER
4. TITLE *(and Subtitle)*: Finite Element Analysis of the Forced Oscillations of Ship Hull Forms	5. TYPE OF REPORT & PERIOD COVERED: Engineer's Thesis; June 1974
	6. PERFORMING ORG. REPORT NUMBER
7. AUTHOR(s): David Arthur Smith, Jr.	8. CONTRACT OR GRANT NUMBER(s)
9. PERFORMING ORGANIZATION NAME AND ADDRESS: Naval Postgraduate School, Monterey, California 93940	10. PROGRAM ELEMENT, PROJECT, TASK AREA & WORK UNIT NUMBERS
11. CONTROLLING OFFICE NAME AND ADDRESS: Naval Postgraduate School, Monterey, California 93940	12. REPORT DATE: June 1974
	13. NUMBER OF PAGES: 102
14. MONITORING AGENCY NAME & ADDRESS *(if different from Controlling Office)*: Naval Postgraduate School, Monterey, California 93940	15. SECURITY CLASS. *(of this report)*: Unclassified
	15a. DECLASSIFICATION/DOWNGRADING SCHEDULE

16. DISTRIBUTION STATEMENT *(of this Report)*

Approved for public release; distribution unlimited.

17. DISTRIBUTION STATEMENT *(of the abstract entered in Block 20, if different from Report)*

18. SUPPLEMENTARY NOTES

19. KEY WORDS *(Continue on reverse side if necessary and identify by block number)*

Added mass
Finite element
Nonlinear

20. ABSTRACT *(Continue on reverse side if necessary and identify by block number)*

A study of the first and second-order, dynamic, ideal fluid effects on the forced, harmonic oscillations of a rigid cylinder in a free surface is presented. The solutions are obtained with a FORTRAN IV computer program based on the finite element method using isoparametric elements.

First-order added mass and damping in heave for a semi-circular and bulb hull form including finite depth effects are presented. Second-order solutions for the semi-circular hull form in heave

DD FORM 1 JAN 73 1473 EDITION OF 1 NOV 65 IS OBSOLETE
S/N 0102-014-6601 |
(Page 1)

SECURITY CLASSIFICATION OF THIS PAGE *(When Data Ente*

(20. ABSTRACT continued)

also including finite depth effects are obtained. The solutions are verified by comparing with existing theory and experiment.

Finite Element Analysis of the Forced Oscillations of Ship Hull Forms

by

David Arthur Smith, Jr.
Lieutenant, United States Navy
B.S., University of Missouri, 1966

Submitted in partial fulfillment of the
requirements for the degrees of

MASTER OF SCIENCE IN MECHANICAL ENGINEERING

and

MECHANICAL ENGINEER

from the

NAVAL POSTGRADUATE SCHOOL
June 1974

ABSTRACT

A study of the first and second-order, dynamic, ideal fluid effects on the forced, harmonic oscillations of a rigid cylinder in a free surface is presented. The solutions are obtained with a FORTRAN IV computer program based on the finite element method using isoparametric elements.

First-order added mass and damping in heave for a semi-circular and bulb hull form including finite depth effects are presented. Second-order solutions for the semi-circular hull form in heave also including finite depth effects are obtained. The solutions are verified by comparing with existing theory and experiment.

TABLE OF CONTENTS

LIST OF TABLES

LIST OF FIGURES

LIST OF SYMBOLS

Symbol	Definition
A	One-half of ship's cross-sectional area
a	Amplitude of ship's motion (sway or heave)
b	Ship's half-beam measured at $y = 0$
C_m, C_d	Added mass and damping coefficients, respectively
c_1	Celerity of first-order gravity wave and Stokes second-order wave
c_2	Celerity of second-order gravity wave from velocity potential $\overline{\phi}^{(2)}$
d	Ship's draft
e_1, e_3, e_5	Real coefficients in Lewis hull form equation
$F(t)$	Total nonlinear ship's exciting force
$F^{(1)}, F^{(2)}$	First and second-order components of F, respectively
$\overline{F}^{(1)}, \overline{F}_s^{(2)}, \overline{F}_d^{(2)}$	Nondimensional first and second-order force coefficients
$F_x^{(1)}, F_y^{(1)}$	Resultant first-order hydrodynamic force acting on the ship (sway or heave, respectively).
$f^{(1)}, f^{(2)}$	First and second-order force amplitudes, respectively.
$f_s^{(2)}, f_d^{(2)}$	Amplitude of second-order static and dynamic components, respectively
g	Acceleration of gravity
G_1, G_2, H_1, H_2	Frequency dependent coefficients
h	Fluid region depth
$\vec{i}, \vec{j}$	Unit vectors in cartesian coordinate

Symbol	Definition
i	The imaginary unit $\sqrt{-1}$
k_1, k_2	First and second-order wave numbers, respectively ($k_i = \sigma/c_i$)
ℓ	One-half of the total arc-length of a symmetric ship hull form
m	Total number of nodes in fluid region finite element mesh
m_a	Added mass
$\vec{n}$	Unit outward normal vector from region R
p	Hydrodynamic overpressure (referred to atmospheric)
$p^{(0)}, p^{(1)}, p^{(2)}$	Zero, first, and second-order components of p
$Q(x,0), P(x,0)$	Asymptotic functional forms
$q(y)$	Function describing mode shape of wave generator
$q_p(y)$	Function describing mode shape of plunger type wave generator
$q_f(y)$	Function describing mode shape of flapper type wave generator
$r_1, r_2, \theta_1, \theta_2$	Moduli and arguments of complex numbers
$R(x,0)$	Function representing second-order Stokes free surface boundary condition
R	The domain of the boundary value problem
S	Boundary of the Region R
S_i	Denotes the ith region boundary
s	Arc-length along ship's hull measured from ship's centerline
t	Time
u, v	x,y components of fluid velocity vector, respectively

Symbol	Definition
$\vec{V}$	Ship's velocity vector
w	Reduced region width
w_{min}	Reduced region width parameter
x,y	Two-dimensional inertial cartesian coordinates
$\bar{x}(s),\bar{y}(s)$	Parametric hull coordinates
x_h,y_h	Functions of time such that $\varepsilon x_h,\varepsilon y_h$ represent ship's harmonic motion in sway and heave, respectively
y_h^*	Complex form of y_h
z_1,z_2,w_1,w_2	Complex numbers
α	Reduced region width parameter
$\gamma^{(1)},\gamma^{(2)}$	First and second-order exciting force phase angles measured with respect to ship's "top dead center" position
δ	Dimensionless frequency parameter ($\delta = \sigma^2 b/g$)
ζ	Complex mapping parameter in Lewis hull form equation
ε	Perturbation parameter ($\varepsilon = a/b$)
$\eta(x,t)$	Wave amplitude measured from $y = 0$
$\eta^{(1)}(x,t),\eta^{(2)}(x,t)$	First and second-order components of $\eta(x,t)$
$\bar{\eta}_\infty^{(1)}$	Dimensionless first-order wave amplitude at infinity
$\bar{\eta}^{(1)},\bar{\eta}^{(2)}$	First and second-order dimensionless wave amplitude coefficients ($\bar{\eta}^{(i)} = \bar{\eta}^{(i)}(x,t)$)
μ_o	Maximum amplitude of wave generator
ξ,η	Cartesian coordinates in ξ,η plane
ρ	Fluid density

Symbol	Definition
σ	Circular frequency of ship's motion
$\Phi(x,y,t)$	Real-valued nonlinear velocity potential
$\Phi^*(x,y,t)$	Real-valued nonlinear velocity potential of a traveling gravity wave
$\Phi^{(1)}, \Phi^{(2)}$	First and second-order components of Φ, respectively
$\Phi^{*(1)}, \Phi^{*(2)}$	First and second-order components of Φ^*, respectively
$\phi^{(1)}, \phi^{(2)}$	First and second-order complex, time-independent velocity potentials, respectively
$\bar{\phi}^{(2)}$	Modified complex, second-order velocity potential
ϕ^t	A known test velocity potential
$\psi^{(2)}$	Second-order, complex Stokes wave velocity potential (time-independent)
$\underset{\sim}{\phi}, \underset{\sim}{\phi}^{(1)}, \underset{\sim}{\phi}^{(2)}$	m x 1 column vector of nodal values of $\phi^{(1)}$ or $\phi^{(2)}$
$\underset{\approx}{H}, \underset{\approx}{D}, \underset{\approx}{Q}$	m x m real, symmetric coefficient matrices
$\underset{\approx}{J}$	Jacobian matrix (2 x 2)
$\underset{\approx}{K}^{(1)}$	Total coefficient matrix (m x m) of the discretized first-order system
$\underset{\sim}{N}$	1 x m row vector of cubic isoparametric shape functions
$\underset{\sim}{N}^e$	1 x 12 row vector of cubic isoparametric shape functions at the element level
$\underset{\sim}{r}^{(1)}, \underset{\sim}{r}^{(2)}, \underset{\sim}{\alpha}, \underset{\sim}{\beta}, \underset{\sim}{\gamma}$	m x 1 column vectors
$\vec{\nabla}$	The vector gradient operator
∇^2	Laplacian operator

ACKNOWLEDGEMENTS

The author wishes to express his deep appreciation to Dr. Robert E. Newton, Professor of Mechanical Engineering, for his advice and perceptive guidance throughout the development of this research. His patience and insight were key factors in the successful conclusion of this work.

The author is indebted to Professor C. J. Garrison and Professor T. Sarpkaya for their helpful discussions during the course of this study.

The W. R. Church Computer Center of the Naval Postgraduate School provided the excellent computer service and technical advice for the numerical solutions.

Finally, the author wishes to thank his wife, Wendy, for her patience, understanding, and encouragement during the time of this research.

I. INTRODUCTION

Naval architects and marine engineers have long been greatly interested in the study of the dynamic fluid response to the forced oscillations of a two-dimensional floating body. The applications of the studies include studying the rigid-body response of the ship due to an incoming wave train, and determining the natural frequency and vibration mode shapes of a ship's structure in connection with propulsion systems design [34].

Marine engineers, in modern times, are concerned with, among other things, the natural frequencies and stability characteristics of floating platforms near a coastline. Also, they are concerned with the related problem of finding the dynamic loads on submerged, moored, or fixed bodies [8].

The modern techniques for solving these types of problems involve seeking the solution of a steady-state, periodic, potential flow problem with a free surface in a fluid of either infinite or finite depth. This problem is made tractable by linearizing the free surface boundary condition.

A. HISTORICAL BACKGROUND

The historical development of potential flow problems involving a free surface with wave motion, and the related problem of the dynamic response of fluids due to the motion of rigid bodies on and under a free surface is lengthy; but of interest. Several authors have reviewed this history in

some detail [3,17,24,31]. The history is repeated in the following in the interest of providing a foundation upon which this author endeavors to add additional information in an attempt to provide a more complete history.

1. First Order Solutions

a. General Potential Theory

The foundation of the modern day theory of fluid motions begins, of course, with the classical works of Newton, Lagrange, Euler, Stokes, and others.

However, in 1879, Lamb [15] provided one of the first complete studies of the theory of wave motions; which he updated five times until 1932. It appears that the next major contribution was made by Havelock [10] in 1929; wherein, he studied the solution of the wave forms created by a wave generator.

The modern beginnings of the study of the interaction of a fluid and a harmonically oscillating rigid body at the free surface start with the work of Lewis [19] in 1929. Lewis studied the determination of added mass with a boundary condition requiring zero pressure at the mean position of the free surface, thus eliminating the effects of frequency of body oscillation and of damping. Lewis considered the high frequency case of the more general problem.

The first work which included the effects of frequency and damping was done by Ursell [38] in 1949. This work solved the problem of a right-circular, semi-immersed cylinder heaving on the free surface of a fluid infinite in

extent. Ursell presented added mass and damping coefficients as a function of frequency. His method of solution involved placing an "infinite" number of singularities of all orders at the intersection of the free surface at rest and the cylinder centerline. The strengths of the sources were determined from the kinematic boundary condition applied on the immersed surface of the cylinder. Grim [9] arrived at a similar solution in 1953.

A period of about ten years passed before any additional work was reported on the subject. There is a rather obvious reason for this time lag. Ursell's solution involved laborious numerical calculations which had to be done by hand. The advent of the digital computer made it feasible to pursue further solutions.

In 1960, Tasai [36] extended the work of Ursell to include roll and sway motions of Lewis forms. At the same time, Porter [30] compared linearized pressure calculations with experimental results, and extended the range of solutions to include other hull forms.

It appears that Yu and Ursell [42] provided the first theoretical study of the effect of finite depth on two-dimensional solutions in 1961. This was followed by additional work by Kim [14] in 1969, who also included finite depth. In the first work, added mass coefficients and the properties of the resultant linear wave were reported. The second work, by Kim, gave added mass and damping coefficients as a function of frequency and depth. Work by Paulling and

Richardson [28] and Paulling and Porter [29] provided some experimental verification of the theory in 1962. Vugts [40], at the Netherlands Research Center in 1968, reported additional extensive, experimental research on seven different ship hull forms.

b. Finite Element Solutions

Zienkiewicz [46], in 1965, provided the first successful application of the finite element method to Poisson's equation. Although the finite element method was originally developed to solve problems in the theory of elastic mediums, Zienkiewicz's work "opened the door" to possible solutions to boundary value problems of many different types, including the solution of fluid flow problems; this follows since Laplace's equation is contained in Poisson's equation.

In the same year (1965), Zienkiewicz, Irons, and Nath [44] first used the finite element method to find added mass. Just as in the case of Lewis and others before, surface waves were excluded from this solution, as well as in subsequent works by Rören [32], Holand [12], Matsuura and Kawakami [22], and Matsumoto [21].

Zienkiewicz and Newton [43] presented the first general theoretical treatment of the fluid-structure interaction problem using the finite element theory in 1969. Their work provided a means of including surface waves and determination of energy loss due to wave propagation. The latter was accomplished by providing a radiation boundary condition. This radiation boundary condition was essential to the

successful modeling of infinite regions under steady-state conditions. In addition, compressibility effects could be included in the analysis.

Chenault [4], in 1970, appears to be the first to apply the finite element analysis developed by Zienkiewicz and Newton to find added mass and damping coefficients as a function of frequency and hull form. The fluid regions he studied were chosen to simulate infinite depth. Some of his results are published in Ref. [23]. Bai [3] also included surface waves in his 1972 analysis of a wide range of problems. His work demonstrated the flexibility of the method by studying, in addition to the problems of Chenault, the additions of sway and roll motions, finite depth, irregular fluid bottom geometry, axisymmetric geometry, and fluid stratification. Bai also provided criteria for properly placing the radiation boundary and developed a new form of the radiation condition for the axi-symmetric case.

The author has extended the studies of Chenault and Bai in the solution of the first-order problems with an improved version of Chenault's computer program. The results are presented later in this work along with results separately reported by Newton, Chenault, and Smith [23].

2. Second Order Solutions

a. General Potential Theory

The origins of the second-order theory of gravity waves begin again with the work of Stokes and his classic solution of nonlinear traveling waves. Others have extended

the work of Stokes, but it appears that a modern version of Stokes' theory was first compiled by Stoker [35] in 1957. The generally accepted terminology associated with Stoker's work is "perturbation theory" which of course has applications in many fields.

Fontannet [5], in 1961, appears to be the first to attempt to use the basic nonlinear perturbation theory as described by Stoker to solve the problem of finding the characteristics of waves generated by a plane wave-maker using Lagrangian coordinates. Ogilvie [25], in 1963, found the first and second-order forces on a fixed or oscillating circular cylinder submerged in a fluid with a free surface. However, his second-order forces were only those due to the first-order solution, and only the time-independent part was reported. Tuck [37] found the second-order forces on a submerged cylinder in a uniform stream in 1965. Salvesen [33] extended Tuck's work to include wing-shaped bodies in his Ph.D. dissertation in 1966.

Lee [17] and Parissis [27] appear to be the first to apply second-order perturbation theory to attempt to solve the fluid-structure interaction potential flow problem with a free surface in 1967. Lee confined his studies to the heaving of floating circular and U-shaped sections, while Parissis studied only the circular shape in heave; both studies were in fluids of infinite extent. These investigations, as well as those previously mentioned, required the development of a fluid-structure second-order boundary

condition (discussed in more detail later) in addition to the free-surface equations compiled by Stoker.

The work of Lee and Parissis was followed by that of Potash [31] in 1970. Potash extended the second-order studies to include the additional degrees of freedom of roll and sway and the attendant coupling between modes of motion. Recently, Garrison [7] completed a second-order solution of the problem of determining the dynamic loads experienced by a "fixed" three-dimensional body due to an incoming wave train. His theory includes submerged and surface-piercing bodies.

All of the second-order solutions previously mentioned used some form of singularity distribution in the flow field. The functional forms of the singular functions used were usually taken from the work of Wehausen and Laitone [41].

b. Finite Element Solutions

The author has been able to find only one solution to the second-order, of the class of problems being discussed, by the finite element method. Allouard and Coudert [2] presented a paper at the International Symposium on Finite Element Methods in Flow Problems in January of 1974. They presented a method of solving problems related to floating bodies in water waves under unsteady-linear or stationary-nonlinear (second-order) conditions.

B. OBJECTIVES OF PRESENT RESEARCH

The experimental studies of Paulling and Porter [29], Paulling and Richardson [28], and Vugts [40], previously mentioned, indicated good agreement with the developed linear theory if the amplitude of motion was small. Potash [31] observed that small variations in amplitude caused large discrepancies between Vugt's experimental results and those of linear theory. Potash [31] has shown that second-order effects become significant at higher frequencies and are more significant when roll and/or sway modes are present. However, he did not examine the effect of finite depth on second-order solutions.

The present work has two primary goals. The first is to determine if the finite element method can be successfully applied to finding solutions to second-order boundary value problems of the type previously described. And, if success is achieved in the first objective, the second major goal is to study the significance of nonlinear effects in heave in water of finite depth.

II. FORMULATION OF THE MATHEMATICAL MODEL

The physical problem is to determine the force required to sustain steady, vertical harmonic motion of a floating cylindric ship hull form. The ship will be considered oscillating in an "ideal" fluid of infinite horizontal extent and arbitrary constant depth.

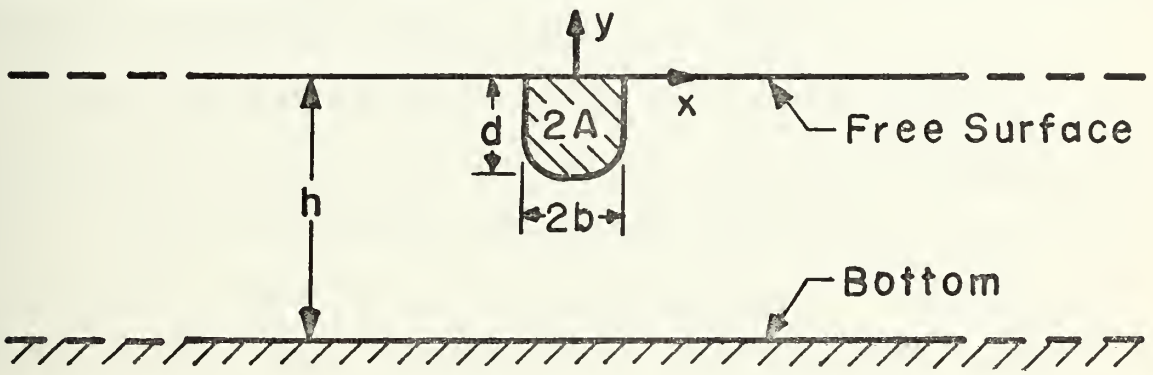

FIGURE 1. Hull at Free Surface

A. THE NONLINEAR BOUNDARY VALUE PROBLEM

The domain of the boundary value problem is shown in figure 1. In the figure, b is the ship's half beam, h is the mean fluid depth, d is the ship's draft, and 2A is the total submerged cross-sectional area of the ship.

The fluid is assumed to be incompressible, inviscid, homogeneous, and without surface tension. It is well known that under the assumption of irrotationality, a velocity potential exists. Furthermore, the potential will be a

single-valued function in any simply-connected region. The convention for the potential used herein is

$$\vec{\nabla}\Phi = u\vec{i} + v\vec{j} \ , \qquad (1)$$

where u is the x-component of fluid velocity, v is the y-component of fluid velocity, and $\vec{i}$ and $\vec{j}$ are the unit vectors in the positive right-handed cartesian coordinate system directions x and y respectively. The symbol $\vec{\nabla}$ is the standard "gradient" used in vector calculus.

The nature of the problem dictates that at a large horizontal distance from the ship's hull (cross-hatched area fig. 1) only an outgoing one-dimensional traveling wave will be present. Therefore, it is advantageous to consider the reduced region shown in figure 2. In figure 2, w is the region semi-width. The meanings of the other symbols shown in figure 2 will become apparent in the following discussion.

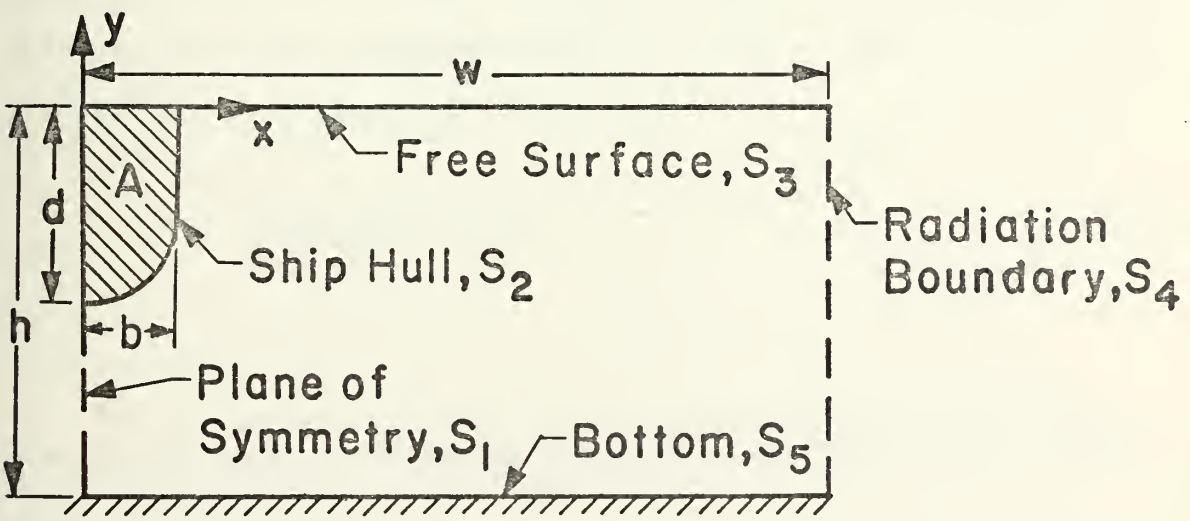

FIGURE 2. Reduced Region

Conservation of mass requires:

$$\nabla^2\Phi = 0 \ , \quad \text{in } R \ . \tag{2}$$

R is the fluid domain and ∇^2 is the Laplacian operator. There are two nonlinear free surface conditions, one dynamic and one kinematic. The dynamic condition, from the Bernoulli equation, is

$$\Phi_t + \frac{1}{2}[\Phi_x^2 + \Phi_y^2] + \frac{p}{\rho} + yg = 0 \ . \tag{3}$$[1]

Equation 3 must hold on the moving free surface ($p = 0$). In the equation, g is the acceleration of gravity, p is the overpressure (referred to atmospheric), ρ is the fluid density, and t is real time. The subscripts denote partial differentiation with respect to the indicated variable. The kinematic condition comes from a basic assumption from continuum mechanics simply stated by Stoker: "A particle once on the free surface remains on it." This assumption translates into the following expression

$$\frac{D[\eta(x,t) - y]}{Dt} = 0 \ . \tag{4}$$

---

[1] In equation 3, the possible pure function of time, which may appear, is assumed to be identically zero without loss of generality (See Stoker [35], p. 10).

Again, equation 4 must be satisfied on the moving free surface. In equation 4, D/Dt denotes the co-moving derivative (sometimes called the substantial or total derivative) and the function $\eta(x,t)$ is defined by the following expression

$$y = \eta(x,t) \quad . \tag{5}$$

Therefore, η is defined to be the wave height above the line $y = 0$ at any point x and any time t.

Equation 4 can be rewritten using the definition of Φ in equation 1 and the definition of the co-moving derivative[2]

$$\Phi_x \eta_x - \Phi_y + \eta_t = 0 \quad , \tag{6}$$

on the moving free surface.

On and "near" the bounding surface S_4 (radiation boundary)

$$\Phi(x,y,t) \to \Phi^*(x,y,t) \quad , \quad \text{as} \quad x \to \infty \quad . \tag{7}$$

In equation 7, Φ^* denotes the velocity potential of a traveling wave moving away from the ship. It must be mentioned here that inherent in the statement of equation 7 is the assumption that the surface S_4 is "far enough" away from the ship's hull. This point will be discussed in more detail later.

Turning to the interface S_2 between the fluid and the ship's hull, the kinematic condition is

---

[2]The co-moving derivative is defined as:

$$D(\ )/Dt \equiv u(\ )_x + v(\ )_y + (\ )_t \quad .$$

$$\vec{\nabla}\Phi \cdot \vec{n} = \vec{V} \cdot \vec{n} \quad . \tag{8}$$

The vector $\vec{n}$ is the unit outward normal vector (from the region R) to the surface at the point of interest. The dot is the standard scalar product and $\vec{V}$ represents the vector velocity of the ship at any instant of time.

Since the motion of the ship is assumed to be restricted to the vertical direction (heave), the bounding surface S_2 becomes a plane of symmetry. The surface S_5, represents the bottom of the fluid region and is rigid. Therefore, both surfaces have the same kinematic boundary condition

$$\vec{\nabla}\Phi \cdot \vec{n} = 0 \quad . \tag{9}$$

An examination of equations 3 and 6 indicates the nonlinearities inherent in the boundary value problem. An additional problem, not as obvious, is the fact that the free surface and the hull are moving boundaries. In its present form the problem has not yielded solutions. Therefore, some approximate theory is applied.

In the development which follows, a perturbation analysis will be applied which when carried to the second-order will produce two linear boundary value problems from the one presently posed. Further, the boundary conditions of both linear problems will be referred to fixed boundaries. In addition, appropriate equations for determining force, and wave profiles will be obtained.

B. PERTURBATION ANALYSIS

First it is assumed that Φ and η each possess a perturbation series representation as follows

$$\Phi = \varepsilon\Phi^{(1)} + \varepsilon^2\Phi^{(2)} + O(\varepsilon^3) , \tag{10}$$

$$\eta = \varepsilon\eta^{(1)} + \varepsilon^2\eta^{(2)} + O(\varepsilon^3) , \tag{11}$$

where ε is a small non-dimensional parameter which is a measure of the size of the ship's motion and is defined as $\varepsilon = a/b$ ("a" is the amplitude of the ship's motion and "b" is the ship's half-beam). Also in equation 10, $\Phi^{(1)}$ and $\Phi^{(2)}$ are defined to be the first and second-order velocity potentials, respectively, and similarly for $\eta^{(1)}$ and $\eta^{(2)}$. Note that as $\varepsilon \to 0$ there is no disturbance and therefore there are no zero-order functions. Substitution of equation 10 into equation 2 yields

$$\varepsilon\nabla^2\Phi^{(1)} + \varepsilon^2\nabla^2\Phi^{(2)} + O(\varepsilon^3) = 0 . \tag{12}$$

Equation 12 implies that

$$\nabla^2\Phi^{(1)} = 0 , \quad \text{and} \tag{13}$$

$$\nabla^2\Phi^{(2)} = 0 , \quad \text{in R} . \tag{14}$$

A similar result holds for equation 9.

1. The Linearized Free Surface Condition

The following development of the linearized free surface conditions follows in general that of Stoker [35]. The final linearized equations for the free surface boundary condition are obtained in the following steps. Equations 5, 10, and 11 are substituted into equation 3, noting that $p_i \equiv 0$ on the free surface. Also, it is observed that $\Phi_t^{(i)}$, $\Phi_x^{(i)}$, and $\Phi_y^{(i)}$ may be represented by the following form of the Taylor series

$$\Phi_\nu(x,y,t) = \Phi_\nu(x,0,t) + \eta(x,t)\Phi_{\nu y}(x,0,t) + \frac{\eta^2}{2}\Phi_{\nu yy}(x,0,t) + O(\eta^3) \quad . \tag{15}$$[3]

After collecting coefficients of like powers of ε in the resulting equation, the following set of equations results

$$g\eta^{(1)} + \Phi_t^{(1)} = 0 \quad , \tag{16}$$

$$g\eta^{(2)} + \Phi_t^{(2)} + \eta^{(1)}\Phi_{ty}^{(1)} + \frac{1}{2}\left[\{\Phi_x^{(1)}\}^2 + \{\Phi_y^{(1)}\}^2\right] = 0 \quad , \quad \text{on } S_3 \ . \tag{17}$$

Applying a very similar procedure to equation 4 yields the following result to the second order

---

[3]The subscript ν denotes partial differentiation with respect to x, y, or t.

$$\eta_t^{(1)} - \Phi_y^{(1)} = 0 \quad , \quad \text{and,} \tag{18}$$

$$\eta_t^{(2)} - \Phi_y^{(2)} + \eta_x^{(1)}\Phi_x^{(1)} - \eta^{(1)}\Phi_{yy}^{(1)} = 0 \quad , \quad \text{on } S_3 \ . \tag{19}$$

Differentiating equation 16 with respect to time, and eliminating η_t from equations 16 and 18 yields the well known linearized free surface condition

$$g\Phi_y^{(1)} + \Phi_{tt}^{(1)} = 0 \quad , \quad \text{on } y = 0 \ . \tag{20}$$

In equation 20, because of the use of the Taylor series expansions in η, the functions are evaluated for $y = 0$, rather than on the actual free surface.
Following the same procedure, as before, for equations 17 and 19 yields

$$g\Phi_y^{(2)} + \Phi_{tt}^{(2)} = \frac{1}{g}\Phi_t^{(1)}(\Phi_{tty}^{(1)} + g\Phi_{yy}^{(1)})$$

$$- 2(\Phi_x^{(1)}\Phi_{xt}^{(1)} + \Phi_y^{(1)}\Phi_{yt}^{(1)}) \ . \tag{21}$$

Note the nonlinear function of $\Phi^{(1)}$ on the right-hand side of equation 21.

2. The Ship Interface Condition

Since the ship boundary is also in "motion", a similar procedure must be applied there to "fix" the boundary S_2. The development follows to some extent that of Potash [31]. Consider figure 3 in which the general ship hull form

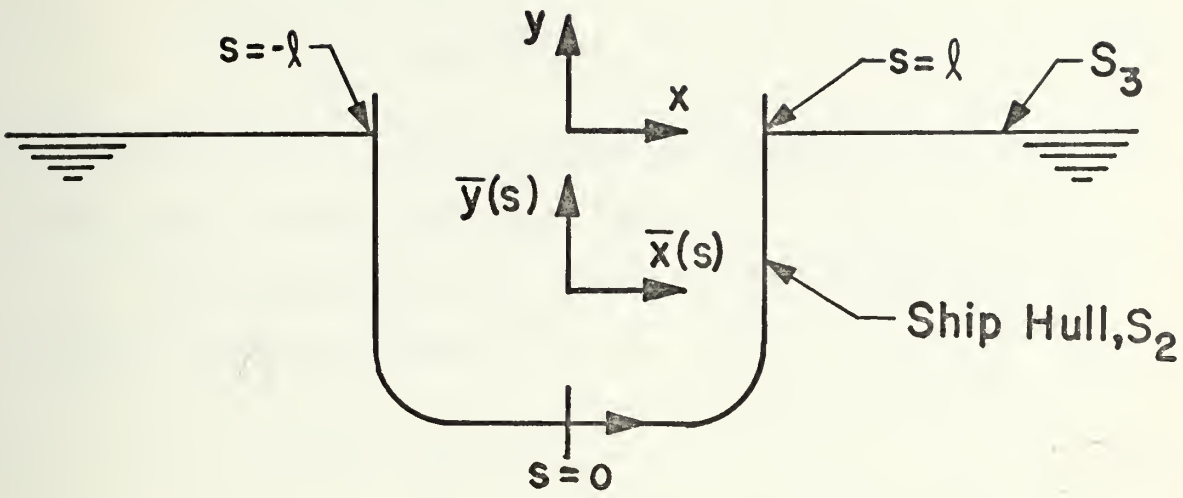

FIGURE 3. Hull Coordinate System

is described in two-dimensional cartesian coordinates in terms of the parameter s (arc length) in the following way

$$\bar{x} = \bar{x}(s) \quad , \quad \bar{y} = \bar{y}(s) \; . \tag{22}$$

The inertial coordinate system is the same as shown in figures 1 and 2. The parametrically represented body coordinates (equation 22) correspond to the inertial coordinates of the body when the ship is at rest (neutrally buoyant position). The motion of the ship in this reference frame can be defined in the following way

$$x(s,t) = \bar{x}(s) \; , \tag{23}$$

$$y(s,t) = \bar{y}(s) + \varepsilon \, y_h(t) \; , \tag{24}$$

where the function y_h is defined to be

$$y_h = \mathrm{Re}\{be^{i\sigma t}\} \ . \tag{25}$$

In equation 25, σ is the circular frequency of the harmonic motion and i is the imaginary unit.

The velocity vector for the ship referred to the inertial reference frame is

$$\vec{V} = \varepsilon \dot{y}_h \vec{j} \ . \tag{26}$$

The dot denotes ordinary time differentiation. The unit outward normal vector (from the region) in terms of the parametric coordinates becomes

$$\vec{n} = -\bar{y}'\vec{i} + \bar{x}'\vec{j} \ , \tag{27}$$

where the prime indicates differentiation with respect to the variable s. Substituting equations 26 and 27 into equation 7 yields the ship-fluid interface boundary condition

$$\vec{\nabla}\Phi \cdot \vec{n} = \varepsilon \dot{y}_h \bar{x}' \ . \tag{28}$$

Now expanding Φ in a Taylor series in ε (similar to free surface expansion) yields

$$\Phi[x(s,t),y(s,t),t] = \Phi(\bar{x},\bar{y},t) + \varepsilon y_h \Phi_y(\bar{x},\bar{y},t) + O(\varepsilon^2) \ . \tag{29}$$

Using equations 10 and 29, the normal derivative of Φ on S_2 may be expressed as

$$\vec{\nabla}\Phi\cdot\vec{n} = (-\bar{y}'\Phi_x^{(1)} + \bar{x}'\Phi_y^{(1)})\varepsilon$$

$$+ [-\bar{y}'\Phi_x^{(2)} + \bar{x}'\Phi_y^{(2)} - \bar{y}'y_h\Phi_{xy}^{(1)} + \bar{x}'y_h\Phi_{yy}^{(1)}]\varepsilon^2 + O(\varepsilon^3) ,$$

$$\text{on } S_2 . \qquad (30)$$

Substituting equation 30 into equation 28 and equating like powers of ε yields the following set of equations valid on the fixed boundary S_2:

$$\nabla\Phi^{(1)}\cdot\vec{n} = \dot{y}_h\bar{x}' , \qquad (31)$$

$$\nabla\Phi^{(2)}\cdot\vec{n} = -\bar{x}'y_h\Phi_{yy}^{(1)} + \bar{y}'y_h\Phi_{xy}^{(1)} . \qquad (32)$$

Equation 32 may also be written

$$\vec{\nabla}\Phi^{(2)}\cdot\vec{n} = -y_h(\vec{h}\cdot\vec{\nabla}\Phi^{(1)})_y . \qquad (33)$$

It remains to consider the boundary S_4 (radiation boundary) and the function Φ^*. For consistency, Φ^* must also be expanded in a perturbation series

$$\Phi^* = \varepsilon\Phi^{*(1)} + \varepsilon^2\Phi^{*(2)} + O(\varepsilon^3) . \qquad (34)$$

Potash [31] and others have shown that $\Phi^{*(1)}$ and $\Phi^{*(2)}$, for a region of infinite depth, each represent a simple harmonic traveling wave of appropriate frequency and wave length. Zienkiewicz and Newton [43] have provided the appropriate homogeneous boundary condition for the surface S_4 to successfully pass a wave form without reflection. The equations are

$$\vec{\nabla}\Phi^{*(1)}\cdot\vec{n} = -\frac{1}{c_1}\Phi^{*(1)}_t \quad , \tag{35}$$

$$\vec{\nabla}\Phi^{*(2)}\cdot\vec{n} = -\frac{1}{c_2}\Phi^{*(2)}_t \quad . \tag{36}$$

In the above equations c_1 and c_2 (the wave celerities) are defined by the following implicit relationships

$$c_1 = (g/\sigma)\tanh\left(\frac{\sigma h}{c_1}\right) \quad , \tag{37}$$

$$c_2 = (g/2\sigma)\tanh\left(\frac{2\sigma h}{c_2}\right) \quad . \tag{38}$$

3. Perturbation Formulas for Pressure, Force and Wave Amplitude

The determination of dynamic loads on the ship requires the following equations which follow from the perturbation series assumed for Φ and η

$$p(x,y,t) = p^{(0)}(x,y) + \varepsilon p^{(1)}(x,y,t) + \varepsilon^2 p^{(2)}(x,y,t) + O(\varepsilon^3) \quad , \tag{39}$$

$$F(t) = \varepsilon F^{(1)}(t) + \varepsilon^2 F^{(2)}(t) + O(\varepsilon^3) \quad . \tag{40}$$

In equation 40, F(t) is defined as the total force per unit length required to sustain simple harmonic vertical translation (see figure 3).

Following a similar procedure as before, evaluating the Bernoulli equation (equation 3) on the ship's hull using equations 23, 24, and 29 yields

$$- \frac{1}{\rho} p[\bar{x}(s),\bar{y}(s),t] = g\bar{y}(s) + \varepsilon[gy_h(t) + \Phi_t^{(1)}(\bar{x},\bar{y},t)]$$

$$+ \varepsilon^2[y_h\Phi_{ty}^{(1)} + \Phi_t^{(2)} + \frac{1}{2}(\{\Phi_x^{(1)}\}^2 + \{\Phi_y^{(1)}\}^2)] + O(\varepsilon^3) \quad . \quad (41)$$

By comparing equation 39 with equation 41 we find

$$p^{(0)} = - \rho g\bar{y}(s) \quad , \quad (42)$$

$$p^{(1)} = - \rho[gy_h + \Phi_t^{(1)}] \quad , \quad (43)$$

$$p^{(2)} = - \rho[y_h\Phi_{ty}^{(1)} + \frac{1}{2}(\{\Phi_x^{(1)}\}^2 + \{\Phi_y^{(1)}\}^2) + \Phi_t^{(2)}] \quad . \quad (44)$$

At this point observe that the second-order pressure is made up of contributions from both the first and second-order potential solutions.

Potash [31] and others have provided relations for the force per unit length acting on the cylinder. However, in this treatment, it is desired to obtain relations for the exciting force as previously defined. The motive is that the theoretical result obtained should correspond to that measured by an appropriate physical experiment. The relation between the exciting force F, harmonic displacement y_h and hydrodynamic pressure p, is

$$F(t) = \varepsilon\rho 2A\ddot{y}_h - \int_{-\ell}^{\ell} p\vec{n}\cdot\vec{j}\, ds \quad , \quad (45)$$

where ℓ is one-half of the total symmetric arc-length of the ship's hull (see figure 3). It should be noted here that Potash [31] has examined the question of the time-dependent total arc-length of the actual wetted hull and its effect on the limits of integration in equation 45. However, it will be stated without proof that, provided the sides of the ship are vertical at y = 0, the second-order effect is zero. The only hull form examined to the second order satisfies this stated requirement. Therefore, equation 45 is exact for the case considered.

In the calculation of the force F, the constant hydrostatic lifting force which comes from $p^{(0)}$ will not be considered since it is not in the definition of F. Accordingly, the following expression for F(t) results using equations 27, 39, 43, 44, and 45

$$F(t) = \varepsilon[\rho 2A\ddot{y}_h - \int_{-\ell}^{\ell} -\rho(gy_h + \Phi_t^{(1)})\bar{x}'\, ds]$$

$$+ \varepsilon^2[-\rho \int_{-\ell}^{\ell} -(y_h\Phi_{ty}^{(1)} + \tfrac{1}{2}[\{\Phi_x^{(1)}\}^2 + \{\Phi_y^{(1)}\}^2] + \Phi_t^{(2)})\bar{x}'\, ds]. \tag{46}$$

Comparing equation 46 with equation 40 yields the following set of equations

$$F^{(1)}(t) = \rho 2A\ddot{y}_h + \rho \int_{-\ell}^{\ell} (gy_h + \Phi_t^{(1)})\bar{x}'\, ds \quad , \tag{47}$$

$$F^{(2)}(t) = \rho \int_{-\ell}^{\ell} [y_h\Phi_{ty}^{(1)} + \tfrac{1}{2}(\{\Phi_x^{(1)}\}^2 + \{\Phi_y^{(1)}\}^2) + \Phi_t^{(2)}]\bar{x}'\, ds \; . \tag{48}$$

The wave amplitude may be written by inspection of equations 16 and 17.

$$\eta^{(1)}(x,t) = -\frac{1}{g}\Phi_t^{(1)} \quad , \tag{49}$$

$$\eta^{(2)}(x,t) = -\frac{1}{g}[\Phi_t^{(2)} + \eta^{(1)}\Phi_{ty}^{(1)} + \frac{1}{2}(\{\Phi_x^{(1)}\}^2 + \{\Phi_y^{(1)}\}^2)] \quad . \tag{50}$$

The boundary value problems for $\Phi^{(1)}$ and $\Phi^{(2)}$ may now be formally stated. However, at this point, a standard separation of variables technique is applied to eliminate time from the solution (since the solution is assumed periodic). The appropriate definitions are

$$\Phi^{(1)}(x,y,t) = \mathrm{Re}\{\phi^{(1)}(x,y)\, e^{i\sigma t}\} \quad , \tag{51}$$

$$\Phi^{(2)}(x,y,t) = \mathrm{Re}\{\phi^{(2)}(x,y)\, e^{i\sigma t}\} \quad . \tag{52}$$

Note the newly defined spatial potential functions $\phi^{(1)}$ and $\phi^{(2)}$ are in general complex. Also because of the definitions in equations 51 and 52 it is necessary to replace y_h by the complex form

$$y_h^* = be^{i\sigma t} \quad . \tag{53}$$

C. THE BOUNDARY VALUE PROBLEM FOR $\phi^{(1)}$

The boundary value for $\phi^{(1)}$ is formally stated using equations 9, 13, 20, 25, 31, and 35.

$$\nabla^2\phi^{(1)} = 0 \ , \quad \text{in } R \ , \tag{54}$$

$$g\phi_y^{(1)} - \sigma^2\phi^{(1)} = 0 \ , \quad \text{on } S_3 \tag{55}$$

$$\vec{\nabla}\phi^{(1)}\cdot\vec{n} = i\sigma b\bar{x}' \ , \quad \text{on } S_2 \tag{56}$$

$$\vec{\nabla}\phi^{(1)}\cdot\vec{n} = \frac{i\sigma\phi^{(1)}}{c_1} \ , \quad \text{on } S_4 \tag{57}$$

$$\vec{\nabla}\phi^{(1)}\cdot\vec{n} = 0 \ , \quad \text{on } S_1 \text{ and } S_5 \ . \tag{58}$$

D. THE BOUNDARY VALUE PROBLEM FOR $\phi^{(2)}$

Similarly, the boundary value problem for $\phi^{(2)}$ may be formally stated using equations 9, 14, 21, 25, 32, and 36.

$$\nabla^2\phi^{(2)} = 0 \ , \quad \text{in } R \ , \tag{59}$$

$$g\phi_y^{(2)} - 4\sigma^2\phi^{(2)} = \frac{i\sigma\phi^{(1)}}{2g}\left[-\sigma^2\phi_y^{(1)} + g\phi_{yy}^{(1)}\right] - i\sigma\left[\{\phi_x^{(1)}\}^2 + \{\phi_y^{(1)}\}^2\right] \ , \quad \text{on } S_2 \tag{60}[4]$$

$$\vec{\nabla}\phi^{(2)}\cdot\vec{n} = \frac{b\bar{y}'\phi_{xy}^{(1)}}{2} - \frac{b\bar{x}'\phi_{yy}^{(1)}}{2} \ , \quad \text{on } S_2 \tag{61}$$

---

[4]The factor ½ on the right-hand side of equations 60 and 61 is due to complex algebra involved and is explained in Appendix A.

$$\vec{\nabla}\phi^{(2)}\cdot\vec{n} = -\frac{2i\sigma\phi^{(2)}}{c_2} \quad , \quad \text{on } S_4 \tag{62}$$

$$\vec{\nabla}\phi^{(2)}\cdot\vec{n} = 0 \quad , \quad \text{on } S_1 \text{ and } S_5 \tag{63}$$

Note the striking similarities between the first and second-order problems. Note also, that the nonlinearities in the original problem have been approximated by the nonlinear terms in $\phi^{(1)}$ in equation 60, and the nonlinear terms in y_h and $\phi^{(1)}$ in equation 61 (y_h does not explicitly appear). The additional nonlinear amplitude dependence comes from ε^2 in the original perturbation expansions (equations 10 and 11). The structure of the problem requires the solution of $\phi^{(1)}$ first in order to define the solution for $\phi^{(2)}$.

The conversion to complex algebra allows another observation to be made. Since only the real part of $\phi^{(1)}$ is meaningful, Appendix A demonstrates the required complex manipulation. Close examination of that result indicates that the nonhomogeneous boundary conditions on $\phi^{(2)}$ contain time-independent terms. This implies $\phi^{(2)}$ has a time-dependent and a time-independent part. However, since the physical quantities of interest in the solution all involve derivatives of $\phi^{(2)}$, the time-independent solution of $\phi^{(2)}$ will not be pursued further.[5] The above comments are also true for the second-order functions of pressure, force, and

---

[5]Lee [18] comments on the time-independent solution in terms of mass transport.

wave amplitude. However, the time-independent quantities are of interest and have physical meaning as will be seen later.

The boundary value problem for $\phi^{(2)}$ is valid only in water of infinite depth. The following discussion will explain the problem and develop a boundary value problem which will allow for the solution of $\phi^{(2)}$ in finite depth.

E. THE SECOND-ORDER BOUNDARY VALUE PROBLEM WITH FINITE DEPTH

Potash [31] has shown that the asymptotic form of the velocity potential Φ as $x \to \infty$ becomes (in water of infinite depth)

$$\Phi(\infty,0,t) = \mathrm{Re}\{\varepsilon G_1 e^{i[\sigma t-(k_1 x+\gamma^{(1)})]} + \varepsilon^2 G_2 e^{i[2\sigma t-(4k_1 x+\gamma^{(2)})]}\}. \tag{64}$$

where k_1 denotes the wave number of the first order wave ($k_1 = \sigma/c_1$) and G_1 and G_2 are coefficients which depend on frequency σ. However in the more general case of finite depth, an additional term due to the Stokes'[6] second-order potential appears as follows

$$\Phi(\infty,0,t) = \mathrm{Re}\{\varepsilon H_1 e^{i[\sigma t-(k_1 x+\gamma^{(1)})]} + \varepsilon^2 [H_2 e^{-i(k_2 x+\gamma^{(2)})} - i\frac{3\sigma}{8c_1^2}\frac{H_1^2\cosh(2k_1h)}{\sinh^2(k_1h)} e^{-2i(k_1 x+\gamma^{(1)})}] e^{2i\sigma t}\} . \tag{65}$$

---

[6] The Stokes potential to the second order is well known to be zero in infinite depth.

In equation 65, k_2 is defined as the second-order wave number ($k_2 = 2\sigma/c_2$). H_1 and H_2 are constants similar to G_1 and G_2. Close examination of equation 65 reveals that the radiation boundary condition (equation 62) would fail since the "Stokes wave" which is present is traveling at the same celerity as the first-order solution. This means that the radiation boundary would "reflect" the Stokes' wave since the boundary condition defined by equation 62 will only pass a wave traveling at a celerity of c_2, defined by equation 38. A successful resolution of the above described difficulty requires the formulation of a different boundary value problem. We define the complex velocity potential $\psi^{(2)}$ as

$$\psi^{(2)} = -\frac{i3\sigma}{8c_1^2} H_1^2 \frac{\cosh[2k_1(y+h)]}{\sinh^2(k_1h)} e^{-2i(k_1x+\gamma^{(1)})} , \qquad (65a)$$

which corresponds to the third term in equation 65. Then, following previous conventions, the complex velocity potential $\overline{\phi}^{(2)}$ is defined as

$$\overline{\phi}^{(2)} = \phi^{(2)} - \psi^{(2)} . \qquad (66)$$

1. The Second-Order Boundary Value Problem for $\overline{\phi}^{(2)}$

The definition of $\overline{\phi}^{(2)}$ in equation 66 allows the formal statement of the following boundary value problem, which follows from equation 66, the definition of $\psi^{(2)}$ and the boundary value problem for $\phi^{(2)}$.

$$\nabla^2 \bar{\phi}^{(2)} = 0 \quad , \quad \text{in } R \ , \tag{67}$$

$$g\bar{\phi}_y^{(2)} - 4\sigma^2\bar{\phi}^{(2)} = i\,\frac{\sigma\phi^{(1)}}{2g}\,[-\sigma^2\phi_y^{(1)} + g\phi_{yy}^{(1)}]$$

$$- i\sigma[\{\phi_x^{(1)}\}^2 + \{\phi_y^{(1)}\}^2] - g\psi_y^{(2)} + 4\sigma^2\psi^{(2)} \quad , \text{ on } S_3, \tag{68}$$

$$\vec{\nabla}\phi^{(2)}\cdot\vec{n} = \bar{y}'\,(\frac{b\phi_{xy}^{(1)}}{2} + \psi_x^{(2)}) - \bar{x}'(\frac{b\phi_{yy}^{(1)}}{2} + \psi_y^{(2)}) \quad , \text{ on } S_2, \tag{69}$$

$$\vec{\nabla}\bar{\phi}^{(2)}\cdot\vec{n} = -\frac{2i\sigma\phi^{(2)}}{c_2} \quad , \quad \text{on } S_4 \quad , \tag{70}$$

$$\vec{\nabla}\bar{\phi}^{(2)}\cdot\vec{n} = -\vec{\nabla}\psi^{(2)}\cdot\vec{n} \quad , \quad \text{on } S_1 \quad , \tag{71}$$

$$\vec{\nabla}\bar{\phi}^{(2)}\cdot\vec{n} = 0 \ , \quad \text{on} \quad S_5 \quad . \tag{72}$$

Equation 70 will now properly behave because the asymptotic form of $\bar{\phi}^{(2)}$ using equations 65 and 66 is

$$\bar{\phi}^{(2)}(\infty,y)\ e^{2i\sigma t} = H_2\ e^{-2i(k_2x+\gamma^{(2)})}\ e^{2i\sigma t} \tag{73}$$

Note the celerity of the complex wave form $\bar{\phi}^{(2)}e^{2i\sigma t}$ is c_2 and the radiation boundary condition will now work.

F. FORMULAS FOR PRESSURE, FORCE, AND WAVE AMPLITUDE

The development which follows requires additional definitions, necessary because of the separation of variables scheme previously introduced. They are:

$$p^{(1)}(x,y,t) = \mathrm{Re}\{\bar{p}^{(1)}e^{i\sigma t}\}\ ,\quad p^{(2)} = \mathrm{Re}\{\bar{p}^{(2)}e^{2i\sigma t}\}, \tag{74}$$

$$F^{(1)}(t) = \mathrm{Re}\{f^{(1)}e^{i\sigma t}\}\ ,\quad F^{(2)}(t) = \mathrm{Re}\{f^{(2)}e^{2i\sigma t}\}\ , \tag{75}$$

$$\eta^{(1)}(x,t) = \mathrm{Re}\{\bar{\eta}^{(1)}(x)e^{i\sigma t}\}\ ,\quad \eta^{(2)} = \mathrm{Re}\{\bar{\eta}^{(2)}(x)e^{2i\sigma t}\}. \tag{76}$$

The functions $\bar{p}^{(1)}$, $\bar{p}^{(2)}$, $\bar{\eta}^{(1)}$, $\bar{\eta}^{(2)}$ are complex. This is also true for the constants $f^{(1)}$ and $f^{(2)}$.

Using the above equations and equations 43, 44, 47, 48, 49, and 50 the equations for pressure, force, and wave height for both first and second-order solutions follow.

$$\bar{p}^{(1)} = -\rho[bg + i\sigma\phi^{(1)}]\ , \tag{77}$$

$$\bar{p}^{(2)} = -\rho[\frac{i\sigma\phi_y^{(1)}b}{2} + \frac{1}{2}(\{\phi_x^{(1)}\}^2 + \{\phi_y^{(1)}\}^2) + 2i\sigma\phi^{(2)}]\ , \tag{78}$$

$$f^{(1)} = -2\rho bA\sigma^2 + \rho\int_{-\ell}^{\ell}(gb + i\sigma\phi^{(1)})\bar{x}'\,ds\ , \tag{79}$$

$$f^{(2)} = -\rho\int_{-\ell}^{\ell}(\frac{i\sigma\phi_y^{(1)}b}{2} + \frac{1}{2}[\{\phi_x^{(1)}\}^2 + \{\phi_y^{(1)}\}^2] + 2i\sigma\phi^{(2)})\bar{x}'\,ds, \tag{80}$$

$$\bar{\eta}^{(1)} = -\frac{i\sigma\phi^{(1)}}{g}\ , \tag{81}$$

$$\bar{\eta}^{(2)} = -\frac{1}{g}\left(2i\sigma\phi^{(2)} + \frac{i\sigma\bar{\eta}^{(1)}\phi_y^{(1)}}{2} + \frac{1}{2}[\frac{\{\phi_x^{(1)}\}^2}{2} + \frac{\{\phi_y^{(1)}\}^2}{2}]\right)\ . \tag{82}$$

Again, equations 78, 80, and 82 include the special consideration of the complex algebra involved which is explained in Appendix A.

III. FINITE ELEMENT DISCRETIZATION

The Finite Element Method and its application to scalar field problems is described in various texts, including one by Zienkiewicz [45]. The essential ideas involved follow. The region of figure 2 is replaced by a grid or mesh of finite elements as shown in figure 4.

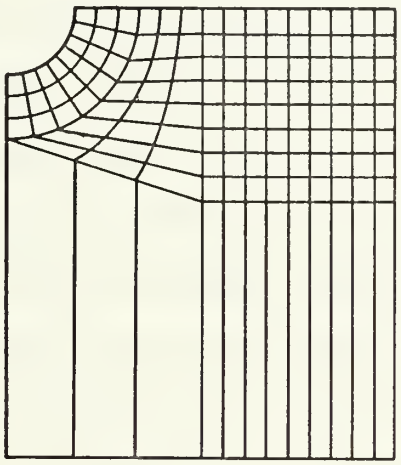

FIGURE 4. Finite Element Mesh

Then it is assumed that the field function sought can be represented by the following equation

$$\phi(x,y) = \underset{\sim}{N}\ \underset{\sim}{\phi} \quad , \quad \text{in } R \ . \tag{83}$$

The total number of nodes in the region will be defined to be m. Then $\underset{\sim}{N}$ is a 1 x m row vector of shape (interpolating) functions and $\underset{\sim}{\phi}$ is an m x 1 column vector of nodal values of the complex potential ϕ (in this problem). Equation 83 implies that knowledge of the vector $\underset{\sim}{\phi}$ defines $\phi(x,y)$ everywhere in R.

There are several choices of shape functions N_i which may be used in equation 83. This work selected the cubic shape functions described by Zienkiewicz [45] as the "serendipity family". The elements used are isoparametric. A brief description of the 12-noded isoparametric elements is given in Appendix B for the unfamiliar reader. The key advantage of the isoparametric element lies in the fact that regions with curved boundaries may be readily represented.

The development that follows defines the set of linear equations which determine the vector $\underset{\sim}{\phi}$ of equation 83.

One general approach to discretization of several types of field problems in finite element analysis is to define a functional whose integral over the domain of the problem is to be minimized. The Calculus of Variations shows that if the Euler equation of the integral to be minimized is the governing equation (i.e., Laplace's Equation) then the two problems are equivalent.[7]

However Zienkiewicz and Newton [43] have shown the discretization may be readily accomplished by applying the Galerkin process. The weight functions are chosen to be the nodal shape functions. Mathematically stated

$$\int_R \underset{\sim}{N}^T(\phi_{xx} + \phi_{yy})\, dR = \underset{\sim}{0} . \qquad (84)$$

---

[7] This statement assumes the same boundary conditions are used.

The superscript T denotes transposition and the function ϕ is considered to be any of the complex potential functions whose solution is sought. Application of the divergence theorem transforms equation 84 into

$$\int_R [\underset{\sim}{N}_x^T \; \underset{\sim}{N}_y^T] \begin{bmatrix} \phi_x \\ \phi_y \end{bmatrix} dR = \int_S \underset{\sim}{N}^T \vec{\nabla}\phi \cdot \vec{n} \, dS \quad , \tag{85}$$

where S denotes the boundary of the region R.

A. THE DISCRETIZED FIRST-ORDER PROBLEM

Application of equations 84 and 85 to the first-order boundary value problem ($\phi^{(1)}$) stated in Chapter II yields the following matrix equation

$$(-\sigma^2 \underset{\approx}{Q}_o + \frac{i\sigma}{c_1} \underset{\approx}{D} + \underset{\approx}{H}) \underset{\sim}{\phi}^{(1)} = i\sigma \underset{\sim}{br}^{(1)} \quad . \tag{86}$$

The definitions of the matrices in equation 86 follow. The matrix $\underset{\approx}{H}$ is m x m, real, symmetric, and defined as

$$\underset{\approx}{H} = \int_R [\underset{\sim}{N}_x^T \; \underset{\sim}{N}_y^T] \begin{bmatrix} \underset{\sim}{N}_x \\ \underset{\sim}{N}_y \end{bmatrix} dR \quad . \tag{87}$$

The matrix $\underset{\approx}{H}$ comes from the integral on the left-hand side of equation 85. The matrix $\underset{\approx}{D}$ is m x m, real, symmetric, and defined by

$$\underset{\approx}{D} = \int_{S_4} \underset{\sim}{N}^T \underset{\sim}{N} \, dS \quad . \tag{88}$$

$\underset{\approx}{D}$ is contributed by the boundary integral on the right-hand side of equation 85 and represents the discretization of the radiation boundary condition (equation 57).

The matrix $\underset{\approx}{Q}_o$ is real, m x m, symmetric and given by

$$\underset{\approx}{Q}_o = \frac{1}{g} \int_{S_3} \underset{\sim}{N}^T \underset{\sim}{N} \, dS \ . \tag{89}$$

$\underset{\approx}{Q}_o$ parallels $\underset{\approx}{D}$ in its origin and represents the contribution from the homogeneous free surface boundary condition (equation 55).

The vector $\underset{\sim}{r}^{(1)}$ is real and defined by

$$\underset{\sim}{r}^{(1)} = \int_{S_2} \underset{\sim}{N}^T \overline{\underset{\sim}{x}}' \, dS \ . \tag{90}$$

The above vector is the discretized ship-fluid interface kinematic boundary condition (equation 56). The surfaces S_1, S_3, S_4, and S_5 have homogeneous boundary conditions and therefore make no contribution to $\underset{\sim}{r}^{(1)}$. It follows that $\underset{\sim}{r}^{(1)}$ is non-zero only at nodes along the ship's hull (surface S_2).

B. THE DISCRETIZED SECOND-ORDER PROBLEM

The problem for $\overline{\phi}^{(2)}$ only will be presented since it contains the solution for $\phi^{(2)}$ in the limit. The boundary value problem for $\overline{\phi}^{(2)}$ yields a linear system of complex equations similar to equation 85.

$$(-4\sigma^2 \underset{\approx}{Q}_o + \frac{2i\sigma}{c_2} \underset{\approx}{D} + \underset{\approx}{H}) \, \underset{\sim}{\overline{\phi}}^{(2)} = \underset{\sim}{r}^{(2)} \ . \tag{91}$$

The right-hand side vector $\underset{\sim}{r}^{(2)}$ in equation 80 receives contributions from the surfaces S_1, S_2 and S_3. Accordingly a further decomposition is necessary:

$$\underset{\sim}{r}^{(2)} = \underset{\sim}{r}_1^{(2)} + \underset{\sim}{r}_2^{(2)} + \underset{\sim}{r}_3^{(2)} \quad . \tag{92}$$

The vectors $\underset{\sim}{r}_i^{(2)}$ are defined below. First to be consistent, the function $\psi^{(2)}$ must be represented in the same way as $\bar{\phi}^{(2)}$

$$\psi^{(2)} = \underset{\sim}{N}\ \underset{\sim}{\psi}^{(2)} \tag{93}$$

Then $\underset{\sim}{r}_1^{(2)}$ becomes, from equations 71 and 85,

$$\underset{\sim}{r}_1^{(2)} = \int_{S_1} \underset{\sim}{N}^T \underset{\sim}{N}\ \underset{\sim}{\psi}_x^{(2)}\, dS \quad . \tag{94}$$

The nodal values of $\underset{\sim}{\psi}_x^{(2)}$ are determined by partial differentiation of the function $\psi^{(2)}$ and then representing the function $\psi_x^{(2)}$ in similar manner as equation 93.

The vector $\underset{\sim}{r}_2^{(2)}$ is defined by equations 69 and 85

$$\underset{\sim}{r}_2^{(2)} = \int_{S_2} \underset{\sim}{N}^T \underset{\sim}{N} \bar{y}' \left[\frac{\underset{\sim}{\phi}_{xy}^{(1)_b}}{2} + \underset{\sim}{\psi}_x^{(2)}\right] dS - \int_{S_2} \underset{\sim}{N}^T \underset{\sim}{N} \bar{x}' \left[\frac{\underset{\sim}{\phi}_{yy}^{(1)_b}}{2} + \underset{\sim}{\psi}_y^{(2)}\right] dS \quad . \tag{95}$$

Similarly $\underset{\sim}{r}_3^{(2)}$ follows from equations 68 and 85

$$\underset{\sim}{r}_3^{(2)} = \frac{1}{g} \int_{S_3} \underset{\sim}{N}^T \underset{\sim}{N} \left[-\frac{i\sigma^3}{2g}\, \underset{\sim}{\alpha} + \frac{i\sigma}{2}\, \underset{\sim}{\beta} - i\sigma \underset{\sim}{\gamma} - g\underset{\sim}{\psi}_y^{(2)} + 4\sigma^2 \underset{\sim}{\psi}^{(2)}\right] dS \quad . \tag{96}$$

The i^{th} component of $\underset{\sim}{\alpha}$ is

$$\alpha_i = \phi_i^{(1)} \phi_{i,y}^{(1)} \tag{97}$$

where $\phi_i^{(1)}$ and $\phi_{i,y}^{(1)}$ are the i^{th} components of $\underset{\sim}{\phi}^{(1)}$ and $\underset{\sim}{\phi}_y^{(1)}$, respectively. Similarly

$$\beta_i = \phi_i^{(1)} \phi_{i,yy}^{(1)} \quad , \text{ and} \tag{98}$$

$$\gamma_i = \{\phi_{i,x}^{(1)}\}^2 + \{\phi_{i,y}^{(1)}\}^2 \quad , \tag{99}$$

The nodal values of the various partial derivatives of $\phi^{(1)}$ are determined by differentiating equation 83. The method of calculation is discussed in the next section. The reader, unfamiliar with isoparametric elements, should refer to Appendix B prior to reading the next section.

1. Calculation of Nodal Values of the Field Derivatives of $\phi^{(1)}$

The vectors $\underset{\sim}{\phi}_x^{(1)}$, $\underset{\sim}{\phi}_y^{(1)}$, $\underset{\sim}{\phi}_{xy}^{(1)}$, and $\underset{\sim}{\phi}_{yy}^{(1)}$ required in equations 95 and 96 are determined by applying standard concepts of finite element analysis. The appropriate relation for the i^{th} node of a given element is

$$\begin{bmatrix} \phi_{i,x}^{(1)e} \\ \phi_{i,y}^{(1)e} \end{bmatrix} = \underset{\approx}{J}^{-1} \begin{bmatrix} \underset{\sim}{N}_\xi^e \\ \underset{\sim}{N}_\eta^e \end{bmatrix} \underset{\sim}{\phi}^{(1)e} \tag{100}$$

$\underset{\approx}{J}$ is the 2 x 2, real Jacobian matrix of the transformation. The vector $\underset{\sim}{N}^e$ is a 1 x 12 row vector of element level shape functions. The superscript "e" denotes all quantities in brackets are at the element level. In equation 100, the elements of $\underset{\approx}{J}^{-1}$ and $\underset{\sim}{N}^e$ are evaluated at node i.

Application of equation 100 to all twelve nodes of a given element determines the vectors $\underset{\sim}{\phi}_x^{(1)e}$ and $\underset{\sim}{\phi}_y^{(1)e}$. Then, replacing $\underset{\sim}{\phi}^{(1)e}$ by $\underset{\sim}{\phi}_y^{(1)e}$ in equation 100 yields the components of the vectors $\underset{\sim}{\phi}_{xy}^{(1)e}$ and $\underset{\sim}{\phi}_{yy}^{(1)e}$. Mathematically stated

$$\begin{bmatrix} \phi_{i,xy}^{(1)e} \\ \\ \phi_{i,yy}^{(1)e} \end{bmatrix} = \underset{\approx}{J}^{-1} \begin{bmatrix} \underset{\sim}{N}_\xi^e \\ \\ \underset{\sim}{N}_\eta^e \end{bmatrix} \underset{\sim}{\phi}_y^{(1)e} \quad . \tag{101}$$

IV. THE COMPUTER PROGRAM AND NUMERICAL SOLUTION

A. MAIN FEATURES OF THE COMPUTER PROGRAM

The formation and solution of the linear system of equations defined by equation 86 ($\phi^{(1)}$ system) or equation 91 ($\phi^{(2)}$ system) was accomplished on an IBM 360/67 computer at the Naval Postgraduate School. The computer has a maximum word length of sixteen bytes.

A comparison of equations 86 and 91 demonstrates the close similarity of the coefficient matrices for the first and second-order solutions. Note that only the coefficients of $\underset{\approx}{Q}_o$ and $\underset{\approx}{D}$ change. An additional observation follows from examination of equations 87, 88, and 89 defining $\underset{\approx}{H}$, $\underset{\approx}{D}$, and $\underset{\approx}{Q}_o$ respectively. Note that all three matrices are purely a function of mesh geometry. Therefore, once a mesh is chosen to define the region of interest, the three matrices previously mentioned need only be calculated once regardless of the forced motion.

A well known property of the finite element method is that it usually produces a banded, symmetric, coefficient matrix. That is the case here and this has obvious computational advantages. However, in this problem, the final system of equations is a function of the frequency of motion as for example in the first-order problem

$$\underset{\approx}{K}^{(1)}\underset{\sim}{\phi}^{(1)} = i\sigma b\underset{\sim}{r}^{(1)} \quad . \tag{102}$$

The matrix $\underset{\approx}{K}^{(1)}$ is an m x m complex matrix defined by equation 86 to be

$$\underset{\approx}{K}^{(1)} = -\sigma^2 \underset{\approx}{Q}_o + \frac{i\sigma}{c_1} \underset{\approx}{D} + \underset{\approx}{H} \quad . \tag{103}$$

Although $\underset{\approx}{K}^{(1)}$ is complex and frequency dependent, it is possible to perform most of the triangular decomposition of $\underset{\approx}{K}^{(1)}$ (by Gauss elimination) only once, using real arithmetic, for a given problem geometry. This economization was first employed by Chenault [4] and is described in more detail in Appendix C. In addition, this author employed a vector storage of the upper triangular portion of $\underset{\approx}{K}^{(1)}$, which greatly reduced the storage requirements of the program. The vector storage scheme made it possible to store only the portions of $\underset{\approx}{K}^{(1)}$ which are non-zero.

The net advantage of employing Chenault's[8] scheme and the compact vector storage was that the system of 733 complex-equations which is generated by the mesh shown in figure 4 could be solved for both the first and second-order problem twenty times in twenty minutes. Further, only ten percent of the total matrix was actually stored and the computer solution was accomplished in core.

---

[8]The Chenault scheme described in Appendix C was developed by Professor R. E. Newton at the Naval Postgraduate School.

B. NUMERICAL SOLUTIONS

The solution of the first-order problem for a given mesh geometry is required before the second-order solution can be obtained. Further, the first-order solution must be highly accurate if a good second-order solution is to be expected. This fact is made more obvious by re-examining equations 68 and 69 in part II.

1. First Order Numerical Solutions

Several first-order problems were solved and closely examined for accuracy. The numerical solutions are presented in part V.

a. Mesh Requirements

One of the primary considerations in choosing a proper mesh concerns the positioning of the radiation boundary (S_4). It may be recalled that the surface S_4 must be far enough away from the ship hull (location of disturbance) so that the local effect of the disturbance has decayed and only an outgoing wave is present. Bai [3] has addressed this question analytically. He has shown that the eigenfunctions associated with the non-propagating velocity field decay exponentially with x. Bai recommends the criterion

$$w_{min} = \alpha h + b \ , \tag{104}$$

where α is a monotonically increasing function of frequency. The range of α is from 1.5 (low frequency) to 3. The values of α were determined based on the decay rate of the most persistent eigenfunction and an attenuation factor of 0.01.

This investigation has found the above criterion somewhat conservative. A value of $\alpha = 2/3$ was found to be adequate for the velocity potential to numerically approach its asymptotic limit for all frequencies studied for the semi-circular hull ($h/b = 6$). Similarly, a value of $\alpha = 9/10$ was found to be adequate for the bulb hull form described in part V ($h/b = 10$) for all frequencies studied. The values of α specified above were determined for the deepest regions studied for each hull form. The region widths used in this case ($w/b = 6$, $w/b = 10$) were found to be more than adequate for shallower depths.

Another requirement on w which tends to restrict its maximum possible value comes from the practical limits on mesh fineness and the resulting computer storage requirements. The mesh must be sufficiently fine to represent properly a traveling surface wave. The finer the mesh, the larger the computer storage requirements and the longer the computer solution time. Therefore, this latter restriction tends to oppose the former one.

Bai [3] used quadratic elements and recommended at least 10 surface nodes per wave length. Visser and Van der Wilt [39] also used quadratic elements and recommended that an element could not span more than one quarter of a wave length. This investigation examined this question in detail. As previously mentioned, cubic isoparametric elements were used. It was found that if the gravity wave did not have to be propagated more than two wave lengths, the elements

could be allowed to span six-tenths of a wave length. However, as in the case Visser and Van der Wilt [39] studied, the successful propagation of a gravity wave over many wave lengths requires a finer mesh spacing. The one quarter wave length Visser and Van der Wilt recommend was found to be a practical upper limit.

A parallel problem to positioning the radiation boundary concerns the location of the bottom (surface S_5) to simulate infinite depth. Comparison of the finite element solutions obtained in this study with analytic solutions based on infinite depth led to the conclusion that a keel to bottom clearance (h - d) of 5b will adequately simulate infinite depth. However, satisfying the classical hydrodynamic requirement that the depth must be at least one-half of a wave length becomes impractical at low frequencies. Ignoring this requirement did not seem to affect solution accuracy.

b. Mesh Data Preparation

The meshes for a given boundary geometry were prepared using a very versatile mesh generator computer program developed by Adamek [1] at the Naval Postgraduate School. This tool greatly expedited mesh preparation. For example, the entire data for the mesh shown in figure 4 (733 nodes, 132 elements) could be generated in twenty seconds. A modification was used to supply accurate values of the nodal coordinates along the ship-fluid interface.

c. Convergence of First-Order Solutions

Convergence of the first-order solutions could not be determined by standard numerical techniques (i.e., mesh refinement) due to computer size limitations. However, the excellent agreement between the first-order solutions obtained in this study and both theory and experiment left no doubt that the solutions were quite good.

2. Second-Order Numerical Solutions

The successful solution of the first-order problem made study of the second-order problem possible.

a. Mesh Requirements

All of the requirements on mesh geometry previously mentioned for the first-order solutions of course apply to the second-order solution. However, the second-order problem demands even more stringent requirements. One reason for this follows from the fact that the wave lengths of the propagating portion of the second-order velocity potential are much shorter (one-fourth of the first-order wave lengths in infinite depth solutions). Therefore, since it is impractical to use a different mesh for each solution, the mesh must have a free surface element spacing approximately one-fourth of that required for the solution of $\phi^{(1)}$ for a given frequency range to be studied. The mesh shown in figure 4 was used to solve the infinite depth second-order problem. It contains 132 elements and 733 nodes.

b. The Second-Order Boundary Condition on S_3

Additional constraints on mesh geometry were found to be required. These constraints arise from the requirements to calculate second-order partial derivatives of $\phi^{(1)}$ which appear in equations 95 and 98. It was essential to have rectangular elements with equal node spacing along the free surface for success in representing the non-homogeneous boundary condition given by equation 96.

The further discussion of this point will be aided by the definitions of some complex functions. Define

$$Q(x,0) = \frac{i\sigma\phi^{(1)}}{2g}\left[-\sigma^2\phi_y^{(1)} + g\phi_{yy}^{(1)}\right] - i\sigma\left[\{\phi_x^{(1)}\}^2 + \{\phi_y^{(1)}\}^2\right] , \tag{105}$$

$$R(x,0) = g\psi_y^{(2)} - 4\sigma^2\psi^{(2)} \quad . \tag{106}$$

In terms of these definitions the right-hand side of equation 68 is

$$P(x,0) = Q(x,0) - R(x,0) \quad . \tag{107}$$

The reader should recall that the successful solution of the boundary value problem for $\phi^{(2)}$ using the method of finite elements required the definition of a new boundary value problem for the function $\bar{\phi}^{(2)}$. The reason was that in the finite depth problem a second-order Stokes' wave is produced with celerity c_1 as well as a second-order wave with celerity c_2 (contained in $\bar{\phi}^{(2)}$). The presence of the two waves with different celerities meant the radiation boundary condition

would fail. The problem was mathematically eliminated by subtracting the well-known analytic solution for the Stokes wave portion of the second-order solution of $\phi^{(2)}$ on <u>every</u> boundary of the region R. The mathematical steps are straightforward as shown in Chapter II. The asymptotic value of the function P(x,0) is zero as x gets large. But, the function R(x,0) which represents the classic Stokes second-order wave free surface boundary condition has the form

$$R(x,0) = \frac{3i\sigma^5}{g^2 \sinh^2 k_1 d} \left|\phi^{(1)}(w,0)\right|^2 e^{-2i(k_1 x + \gamma^{(1)})} , \quad (108)$$

everywhere on S_3. Therefore, if the <u>numerical</u> representation of the function P(x,0) is to approach zero near the radiation boundary; the numerical representation of the function Q(x,0) must approach R(x,0) or

$$Q(x,0) \to R(x,0) \quad \text{as} \quad x \to \infty \quad (109)$$

Note that the amplitude and phase of $\phi^{(1)}$ must be known to completely define R(x,0) and therefore $\psi^{(2)}$.

The above discussion points out the necessity of a very accurate numerical determination of the function Q(x,0). The second-order solutions for $\overline{\phi}^{(2)}$ were closely examined near the radiation boundary and it was found that on the average the function Q(x,0) was within one-percent of the analytic function R(x,0). This accuracy was achieved even though formation of Q(x,0) requires calculation of second derivatives

of $\phi^{(1)}$ using element shape functions which guarantee only C^0 continuity <u>across</u> inter-element boundaries.

c. The Ship-Fluid Interface Second-Order Boundary Condition

The accurate representation of the ship-fluid interface (S_2) boundary condition for the second-order boundary value problem (equation 69) is of course essential. Potash [31] encountered difficulties in making a numerical calculation on this boundary because the potential singularities which define his solution lie along S_2. This results in the required functions $\phi_{xy}^{(1)}$ and $\phi_{yy}^{(1)}$ being only piecewise continuous. This problem required an additional approximation to be made.

The method used herein also has the problem that $\phi_x^{(1)}$, $\phi_y^{(1)}$, $\phi_{xy}^{(1)}$, and $\phi_{yy}^{(1)}$ are not continuous across element boundaries. However, no singularities are present. Extensive investigations in this work have shown that it is essential that the elements along the hull be as square as possible, and further that the node spacing on the elements along the hull should be uniform. It was found that if the hull elements were distorted (not square or rectangular) the numerical representation of the functions $\phi_{xy}^{(1)}$ and $\phi_{yy}^{(1)}$ was highly unstable. However, the mesh requirements for numerically calculating $\phi_x^{(1)}$ and $\phi_y^{(1)}$ along the hull were much less stringent.

The adequacy of the hull elements used in this investigation (see figure 4) was tested by defining a known

potential function on the elements along S_2

$$\phi^t = \frac{1}{2} y^2 + i\, xy \tag{110}$$

and then applying the computer program's numerical scheme to calculate the functions ϕ^t_{xy} and ϕ^t_{yy}. Observe that

$$\phi^t_{xy} = i \quad , \tag{111}$$

and

$$\phi^t_{yy} = 1 \ . \tag{112}$$

It was found that the cubic, isoparametric elements along S_2 produced an average error of about one percent in calculating the functions ϕ^t_{xy} and ϕ^t_{yy}. The maximum error observed was five percent at isolated nodes.

d. Convergence of Second-Order Solutions

Again, computer capacity limitations prevented the application of systematic mesh refinement to determine convergence of the second-order solutions. However, it was possible to refine the elements next to the ship's hull and no significant change in the solutions was observed (the elements along the free surface were performing properly). Further, it is shown in Chapter V that second-order results for infinite depth are in satisfactory agreement with those of other researchers. No comparison is available for finite depth solutions, but a smooth transition is observed as the depth becomes effectively infinite (See Chapter V).

V. NUMERICAL RESULTS

A. DEFINITIONS

The definitions which follow are useful for presentation of results.

1. Added Mass and Damping Coefficients

The complex amplitude $F_y^{(1)}$ of the first-order resultant hydrodynamic force acting vertically on the ship's hull is

$$F_y^{(1)} = \int_{-\ell}^{\ell} \bar{p}^{(1)} \bar{x}' \, ds \ . \tag{113}$$

The real part of $F_y^{(1)}$ is in phase with ship's acceleration and the ship's added mass is defined by

$$m_a = \frac{\mathrm{Re}\{F_y^{(1)}\}}{\sigma^2 a} \ , \tag{114}$$

where the ship's acceleration amplitude is given by $\sigma^2 a$. The added mass coefficient is defined to be the ratio of added mass to ship's displaced mass

$$C_m = \frac{m_a}{2\rho A} = \frac{\mathrm{Re}\{F_y^{(1)}\}}{2\rho A a \sigma^2} \ . \tag{115}$$

The imaginary part of $F_y^{(1)}$ is in phase with the velocity of the ship and is the "non-conservative"[9]

---

[9]The potential theory is, of course, conservative. However, the waves which propagate to "infinity" represent work done by the ship which is effectively lost.

component. Accordingly, the damping coefficient is defined to be

$$C_d = \frac{-\mathrm{Im}\{F_y^{(1)}\}}{2\rho A a \sigma^2} \quad . \tag{116}$$

C_m and C_d are frequency dependent for a given hull form and region depth.

A dimensionless frequency parameter is defined as follows

$$\delta = \frac{\sigma^2 b}{g} \quad . \tag{117}$$

The parameter δ is commonly used by other researchers and is used herein for ease of comparison of solutions. The parameter δ is equivalent to $\frac{2\pi b}{\lambda}$ in infinite depth (λ is the wave length).

The added mass and damping coefficients previously defined are for heave. The same coefficients for sway motion are similarly defined. The only difference in the definitions is $F_y^{(1)}$ is replaced by the horizontal force amplitude $F_x^{(1)}$ defined by

$$F_x^{(1)} = - \int_{-\ell}^{\ell} \bar{p}^{(1)} \bar{y}' \, ds \quad , \tag{118}$$

where $\bar{p}^{(1)}$ is the hydrodynamic pressure due to the swaying motion. There is a coupling between sway and rolling motion for a general ship cross-section. However, the only hull form studied in the sway mode was semi-circular in

cross-section and the coupling force for this case is zero. Therefore, the appropriate coefficients typically used are not defined herein.

One further comment is warranted here. The second-order time-dependent hydrodynamic forces are harmonic with frequency 2σ. Therefore the definition of second-order added mass and damping coefficients is meaningless.

2. Dimensionless Force Coefficients

The force coefficients $f^{(1)}$ and $f^{(2)}$ are also presented in dimensionless form. The non-dimensionalizing factor for the various force amplitudes is $1/\rho g b^2$. Table I presents the correspondence between the dimensional and non-dimensional force quantities. The second-order quantities $f_s^{(2)}$ and $f_d^{(2)}$ which appear in table I are amplitudes of the time-independent (static) and time-dependent (dynamic) portions of $f^{(2)}$ respectively. The existence of $f_s^{(2)}$ is readily verified by examining equations 75 and 80 in light of the discussion in Appendix A.

TABLE I
DIMENSIONLESS FORCE COEFFICIENTS

Force Amplitude	$f^{(1)}$	$f_s^{(2)}$	$f_d^{(2)}$
Dimensionless Force Amplitude	$\bar{F}^{(1)}$	$\bar{F}_s^{(2)}$	$\bar{F}_d^{(2)}$

3. Wave Amplitude at Infinity

Another suitable measure of the damping of ship's motion (to the first-order) is the wave amplitude at "infinity" (i.e., near the radiation boundary). Further, experimentally it has been found to be an easier quantity to measure (particularly for high frequency motion since the damping force is very small then). Accordingly, the dimensionless first-order wave amplitude at infinity is defined by

$$\bar{\eta}_{\infty}^{(1)} = \frac{|\bar{\eta}^{(1)}|_{x=w}}{a} \tag{119}$$

B. HULL FORMS

Other investigators have studied a variety of hull forms both by experiment and analytically. The semi-circular hull was chosen because of the wealth of data available for comparison of both first and second-order solutions. The bulb-shaped hull studied by Paulling and Porter [29] was also examined for first-order solutions. The shape of the bulb hull in comparison to the semi-circular hull is shown in figure 5.

The coordinates of the bulb hull studied are defined by the following mapping

$$\bar{x} + i\bar{y} = \zeta + \frac{e_1}{\zeta} + \frac{e_3}{\zeta^3} + \frac{e_5}{\zeta^5} \quad . \tag{120}$$

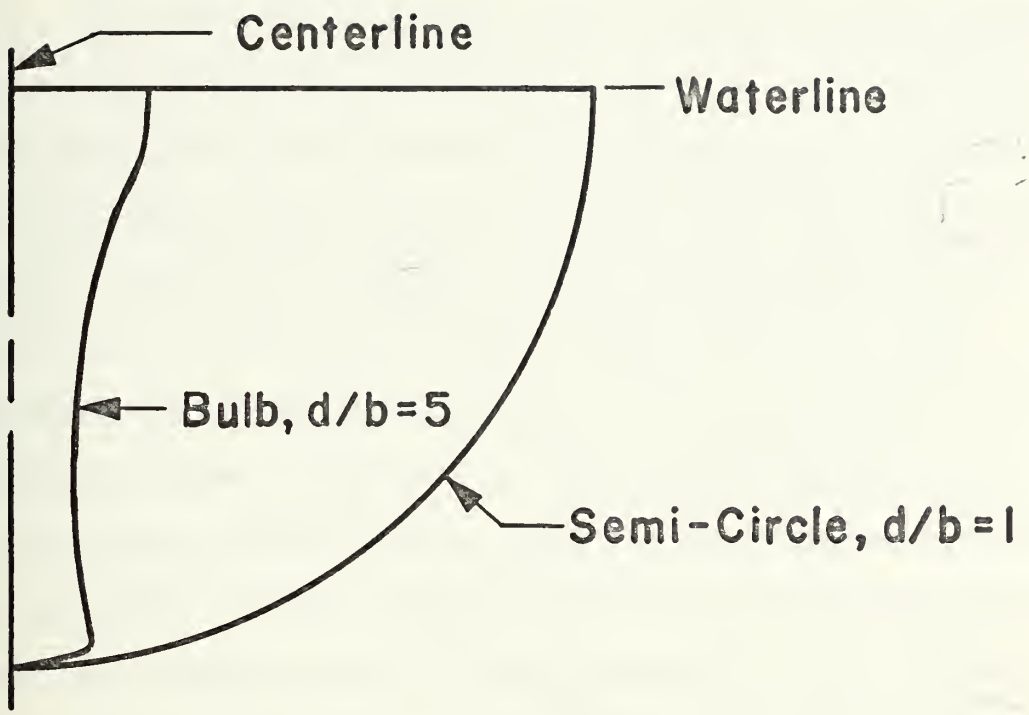

FIGURE 5. Hull Forms

The complex number ζ represents the points on a circle in the ζ-plane. The choice of radius in the ζ-plane defines the scale of the hull cross-section. The values of the e_i are given in table II.

TABLE II
CONSTANTS FOR HULL FORMS

Hull	e_1	e_3	e_5	A/bd
Semi-Circular	0.0	0.0	0.0	0.7854
Bulb	-0.7132	-0.02096	0.0605	0.6950

C. FIRST-ORDER NUMERICAL SOLUTIONS

1. Semi-Circular Hull

The semi-circular hull form has been studied by many researchers mentioned previously in part I. Specifically, the original solution by Ursell [38] for heaving motion has been confirmed analytically by Porter [30], Vugts [40], and others. Ursell's solution has also been experimentally confirmed by Paulling and Porter [29] and Vugts. The analytic results of Ursell for C_m and C_d are shown by the continuous curve in figure 6. The numerical results obtained by the finite element method (FEM) in this work are represented by the circled points in figure 6. The FEM points shown were obtained using a mesh similar to that shown in figure 4, but using only 62 cubic elements and 359 nodes.

The extension of the solutions for C_m and C_d to finite depth is easily accomplished by simply redefining the mesh geometry (decreasing the vertical dimension). Kim [14] and Yu and Ursell [42] reported analytic results. The results obtained by the FEM in this work for $h/d = 4$ agree with those reported by Kim for C_m and $\bar{\eta}_\infty^{(1)}$ within three percent over the range $0.25 < \delta < 5$. The results of Kim are in disagreement with those obtained by Yu and Ursell for $h/d = 2$. The results obtained herein fall between the two. Bai [3] reports inability to verify Kim's result, but gives no details. Bai used the finite element method to obtain his solutions as mentioned in part I.

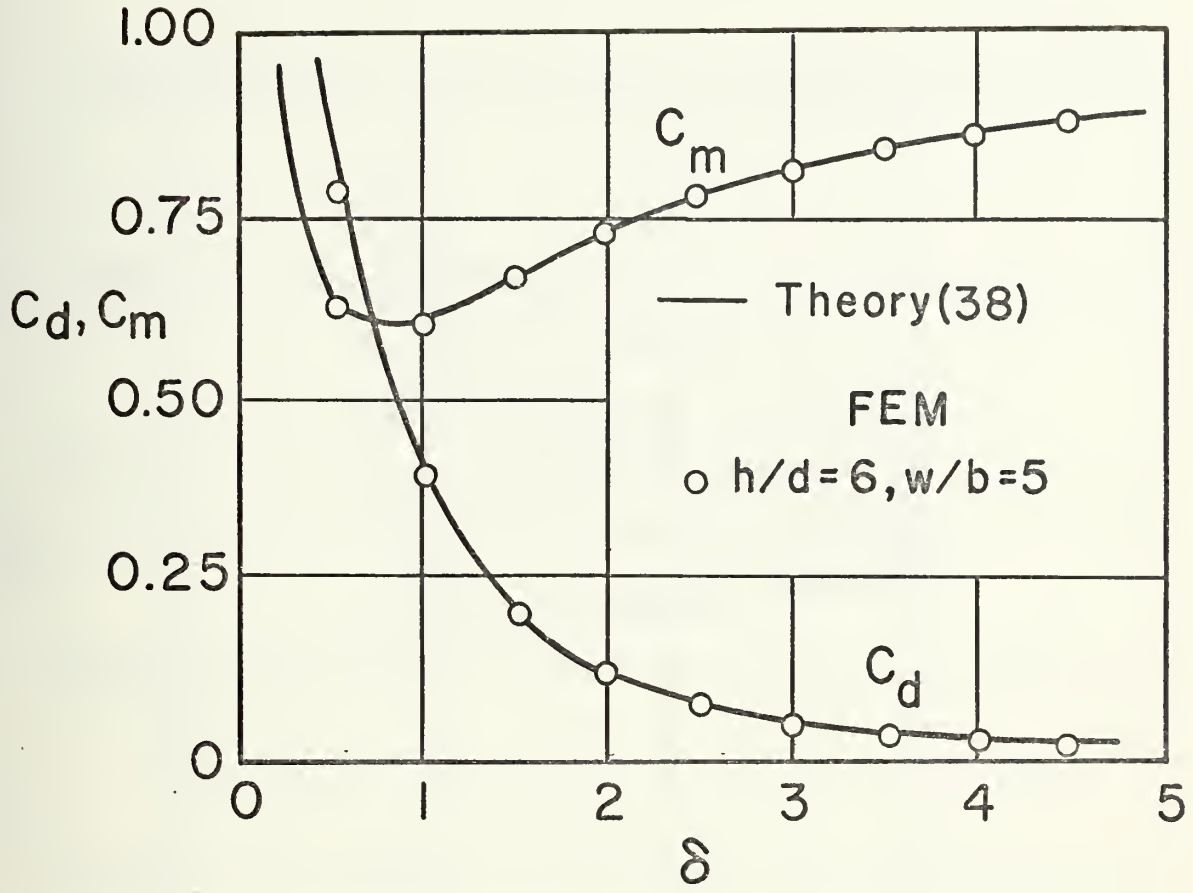

FIGURE 6. Added Mass and Damping Coefficients in Heave, Semi-Circular Hull, Infinite Depth

Figure 7 shows the effect of finite depth on C_m obtained in this work. The figure shows that significant changes do not occur until very shallow water is encountered ($h/d \leq 2$). Further, the effect of shallow water on C_m is more pronounced at very low and very high values of δ. Note the unusual variation with depth for $\delta = 0.5$. C_m decreases with decreasing depth (opposite the trend at higher values

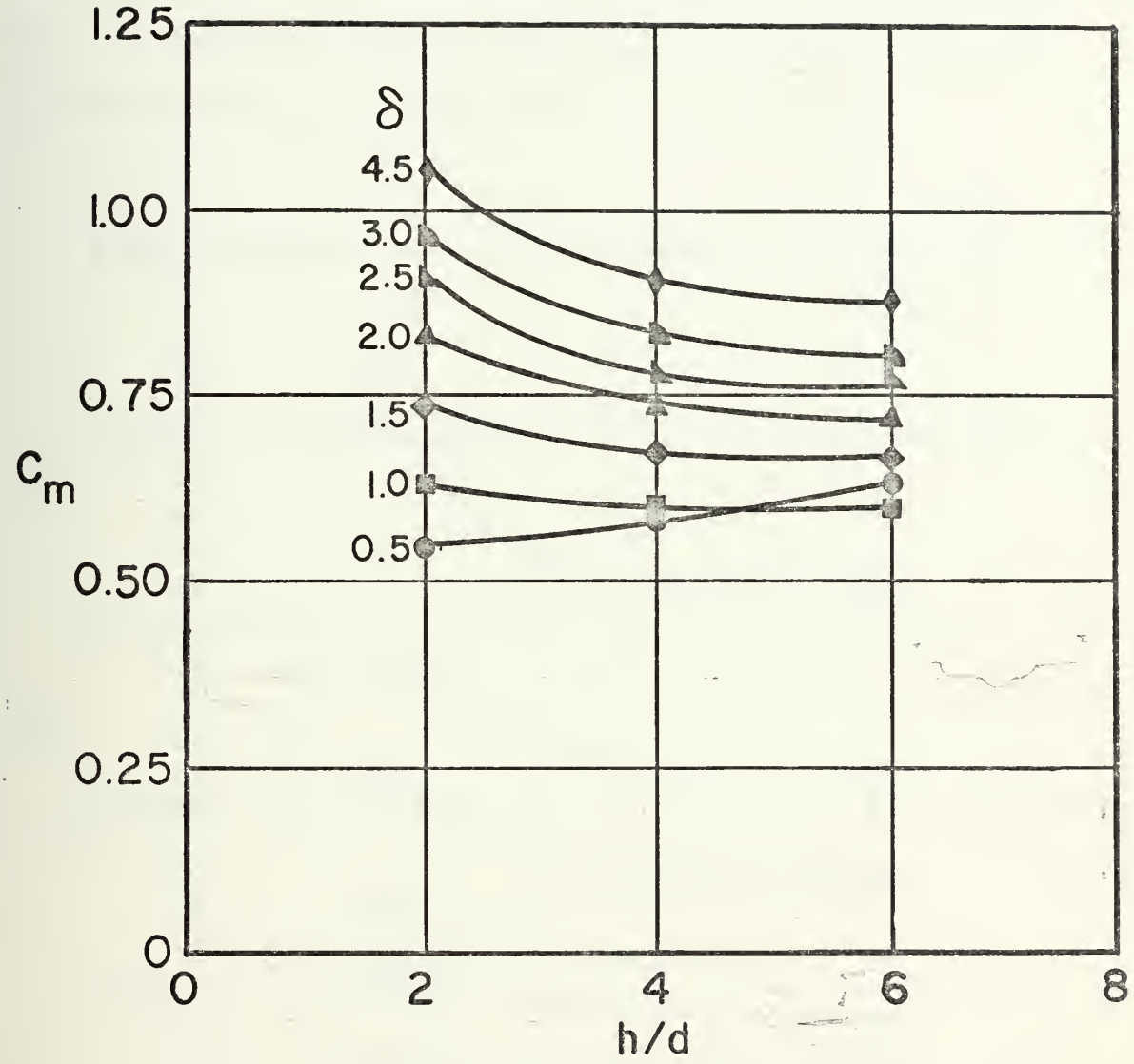

FIGURE 7. Variation of Added Mass Coefficient with Depth, Semi-Circular Hull in Heave

of δ). Although it does not appear true in figure 7, C_m (for δ = 0.5) has reached its asymptotic value at h/d = 6. Figure 8 shows the corresponding effect of finite depth on C_d. The figure indicates that C_d is only sensitive to shallow water effects at very low values of δ.

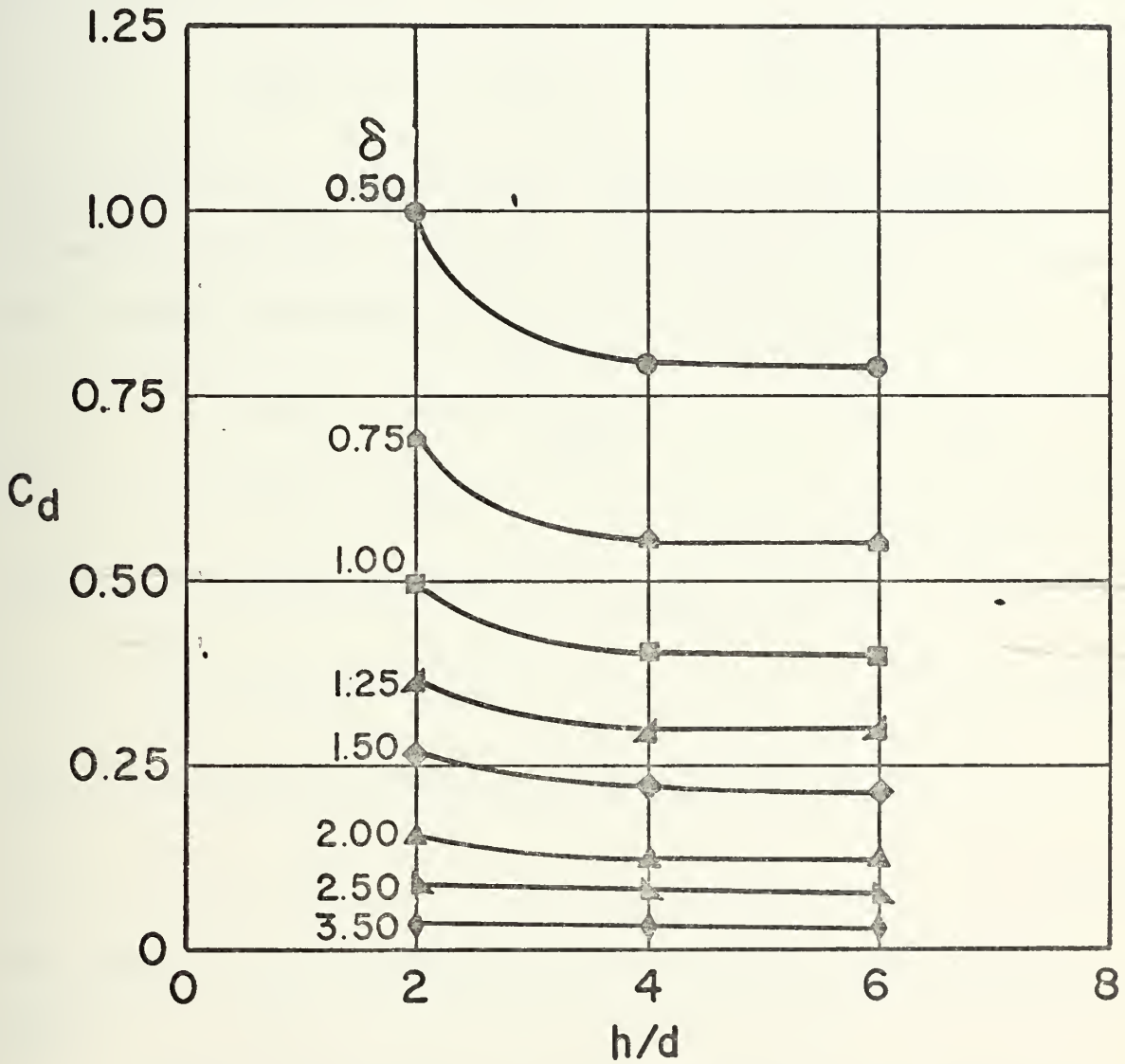

FIGURE 8. Variation of Damping Coefficient with Depth, Semi-Circular Hull in Heave

The semi-circular hull was also studied in sway motion to the first-order. The only changes in the boundary value problem for $\phi^{(1)}$ defined in part II are in equation 56 which defines the surface S_1. The changes are

$$\vec{\nabla}\phi^{(1)}\cdot\vec{n} = i\sigma b\bar{x}' \quad , \quad \text{on } S_2 \quad , \tag{121}$$

for equation 56, and

$$\phi^{(1)} = 0 \quad , \quad \text{on } S_1 \quad , \tag{122}$$

for equation 58. The boundary condition on S_5 defined by equation 58 remains unchanged. The ship's motion is defined in a manner analogous to equations 23 and 24

$$x(s,t) = \bar{x}(s) + \varepsilon\, x_h(t) \quad , \tag{123}$$

$$y(s,t) = \bar{y}(s) \quad . \tag{124}$$

The function $x_h(t)$ is defined the same as $y_h(t)$

$$x_h = \mathrm{Re}\{be^{i\sigma t}\} \quad , \tag{125}$$

and ε is defined in the case of sway motion to be

$$\varepsilon = \frac{a}{b} \tag{126}$$

The symbol "a" is the amplitude of the sway motion in this case.

Vugts [40] presents both experimental and analytic solutions for C_m and C_d for the semi-circular hull in sway. Figure 9 shows a comparison of Vugts' theoretical solution

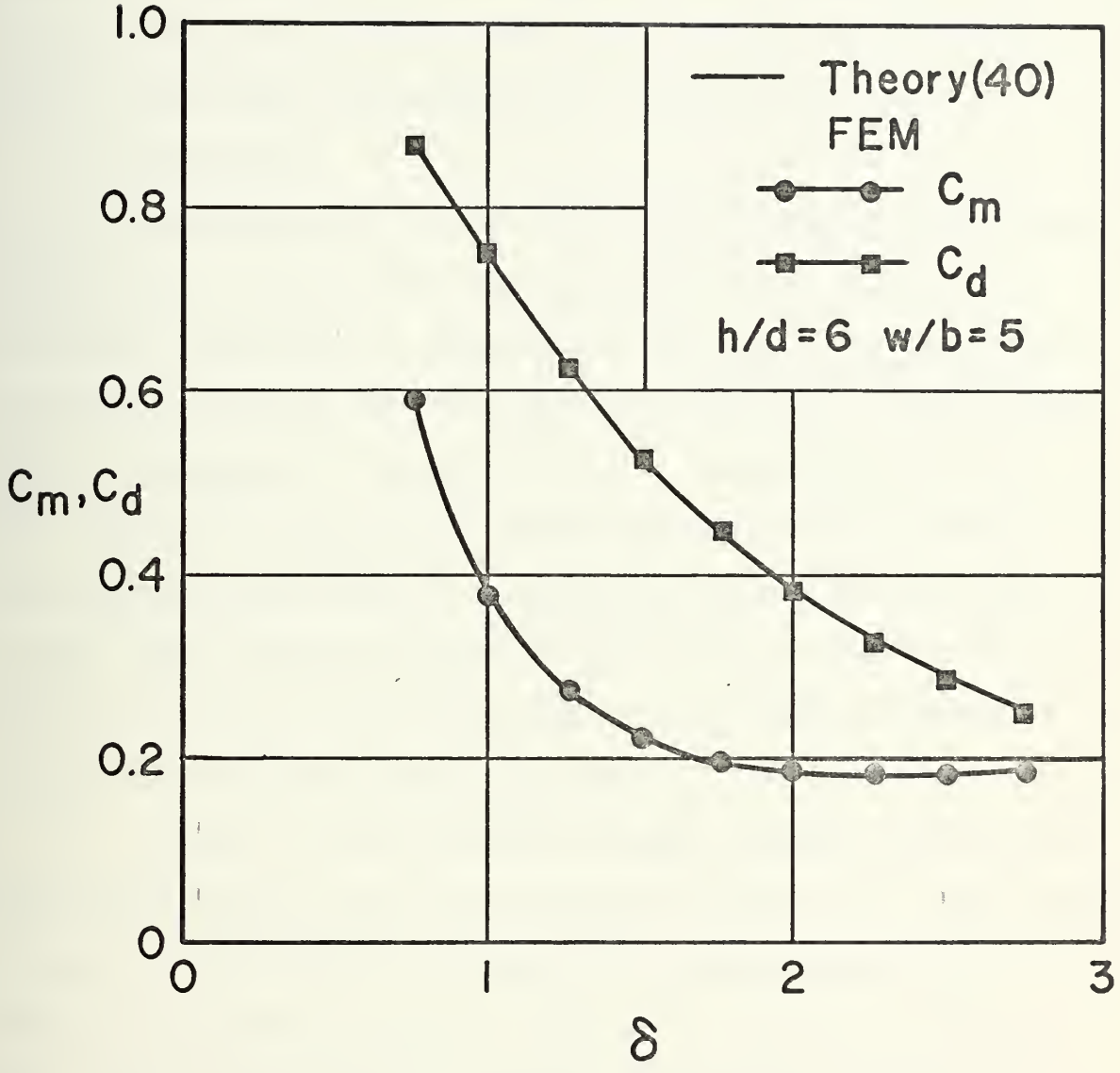

FIGURE 9. Added Mass and Damping Coefficients in Sway, Semi-Circular Hull, Infinite Depth

with the FEM results obtained herein. The FEM calculated points are shown by the solid circles and squares in the figure. The solid curve (from Vugts' theory) was scaled from a very small graph and may be somewhat in error.

2. Bulb Hull

Paulling and Porter [29] reported both analytic and experimental results for the bulb hull form. They show excellent agreement by comparing first-order exciting force amplitude coefficients $\bar{F}^{(1)}$ and wave amplitude coefficients $\bar{\eta}_{\infty}^{(1)}$ respectively. Figures 10 and 11 compare the values of $\bar{F}^{(1)}$ and $\bar{\eta}_{\infty}^{(1)}$ obtained by the FEM herein (circled points) and Paulling and Porter's theoretical calculations (solid line). The FEM mesh parameters were h/d = 2 and w/b = 25. This value of w/b was found later to be quite conservative (w/b = 10 would have been adequate).

Figure 12 shows added mass and damping coefficients for the bulb hull vs h/d for various values of δ. The curves have a similar trend to those of the semi-circular hull form. The corresponding curves of force $\bar{F}^{(1)}$ and wave amplitude $\bar{\eta}_{\infty}^{(1)}$ are not presented. However, the maximum change in exciting force amplitude does not exceed five percent for h/d = 1.2 as compared to infinite depth (h/d = 2). Similarly, the maximum change in $\bar{\eta}_{\infty}^{(1)}$ was only ten percent over the same range of h/d.

3. Wave Generator Studies

MacCamy [20], in 1957, reported an analytic theory using a Green's function approach for solving the problems

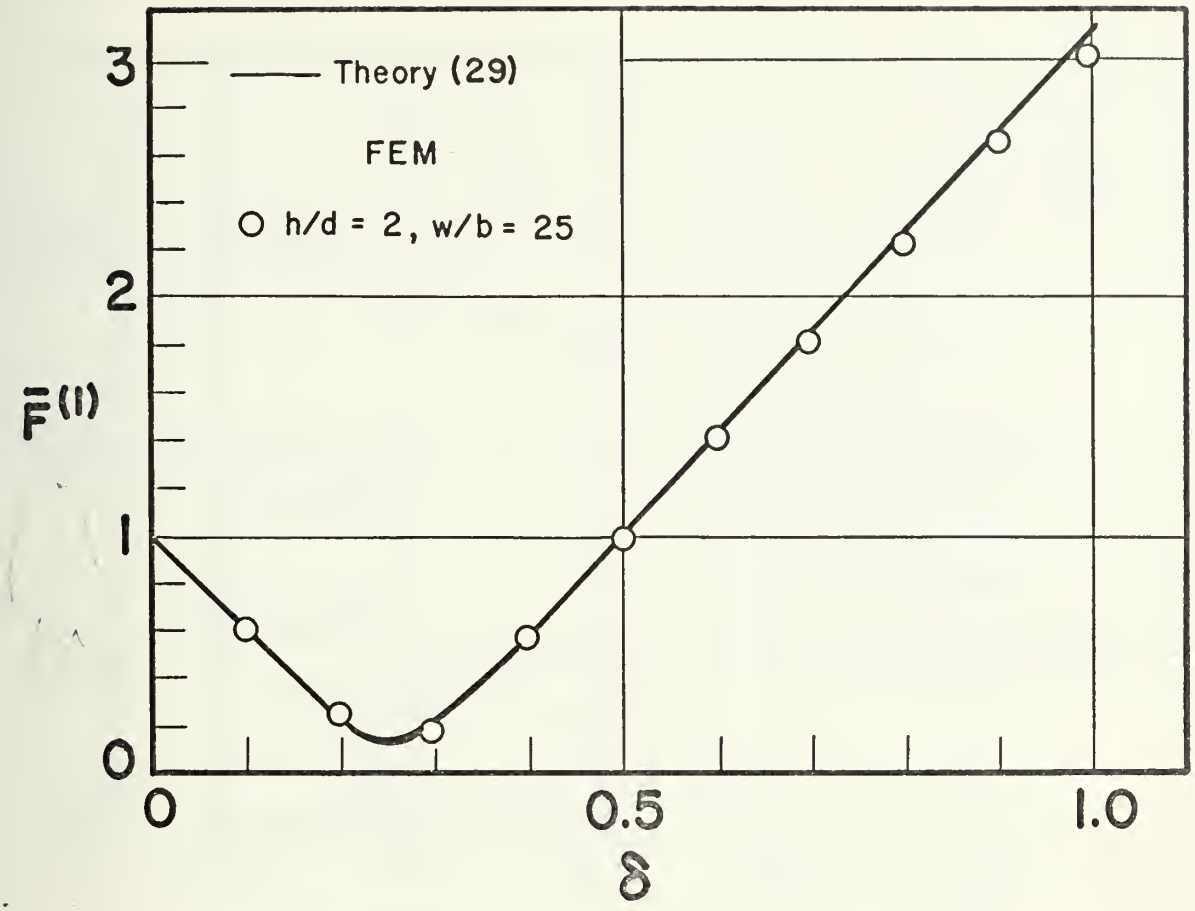

FIGURE 10. Exciting Force Amplitude in Heave, Bulb Hull, Infinite Depth

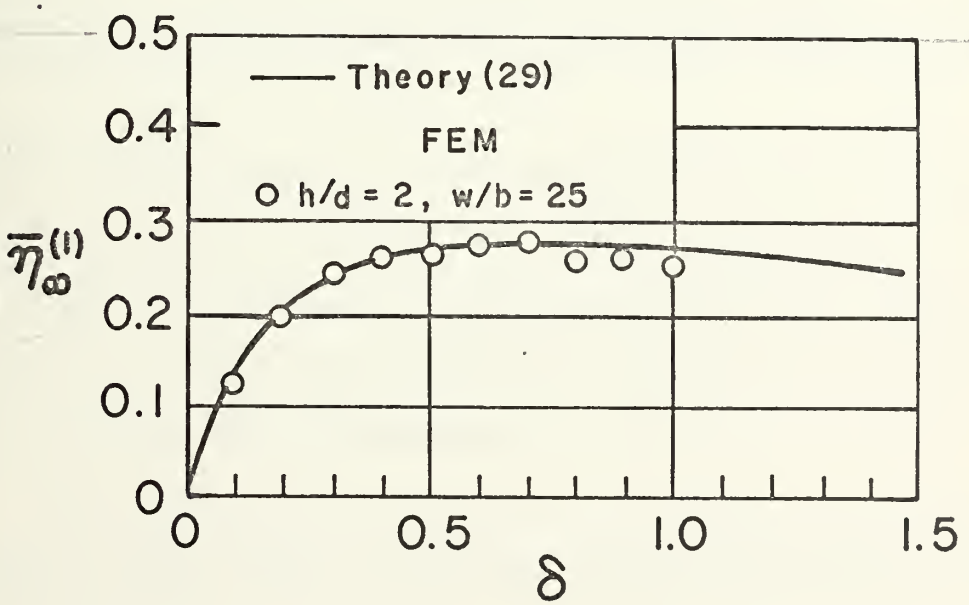

FIGURE 11. Wave Amplitude for Heave, Bulb Hull, Infinite Depth

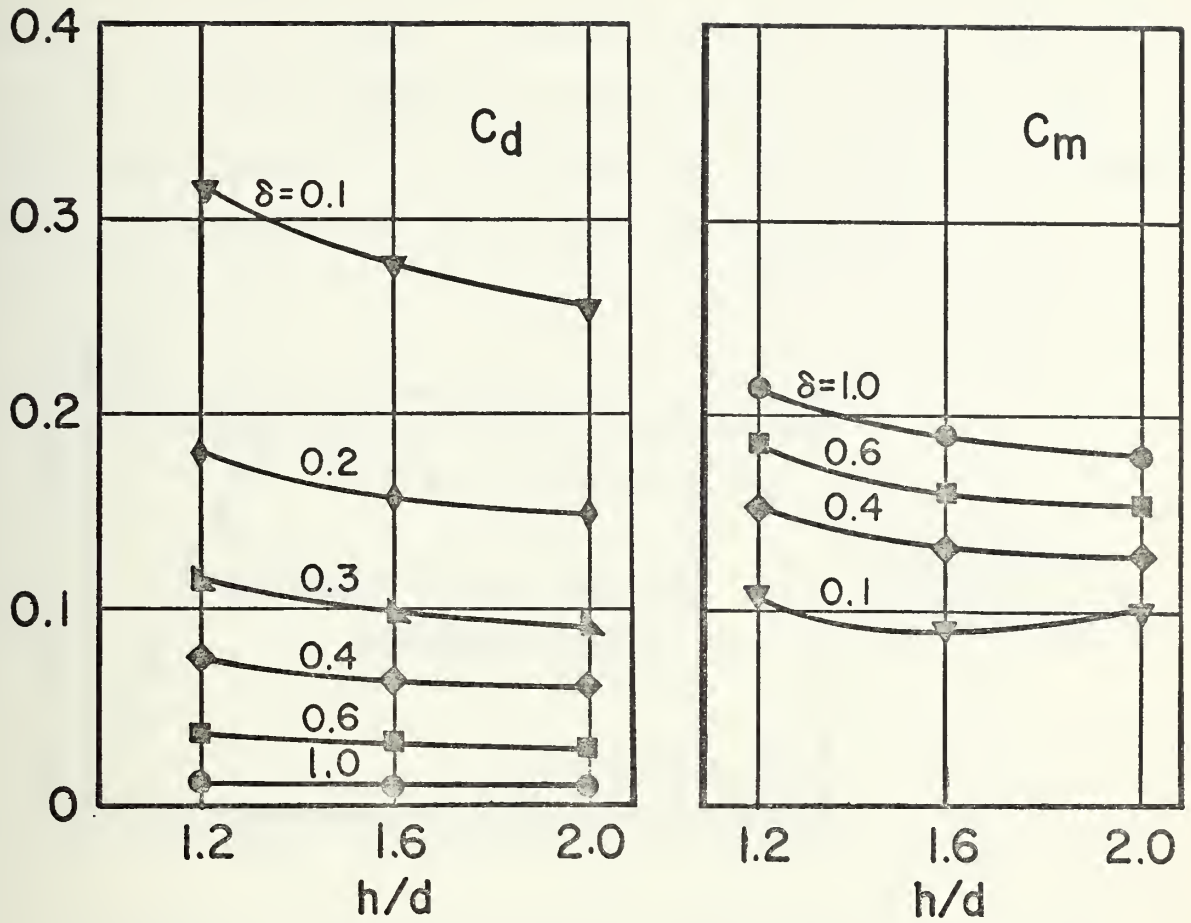

FIGURE 12. Variation of Added Mass and Damping Coefficients with Depth, Bulb Hull in Heave

of gravity wave production by a moving partition and gravity wave reflection from a horizontal strip. The problem of gravity wave production by a moving partition was studied in this work to further help determine proper mesh characteristics for gravity wave propagation.

The wave generation problem is readily placed in the framework of the class of problems being studied herein with

only minor modifications.[10] All of the boundary conditions posed for $\phi^{(1)}$ in part II remain unchanged except those on S_1 and S_2. The surfaces S_1 and S_2 become a vertical line. The region therefore is rectangular. The left-hand boundary will be designated as S_1' as shown in figure 13.

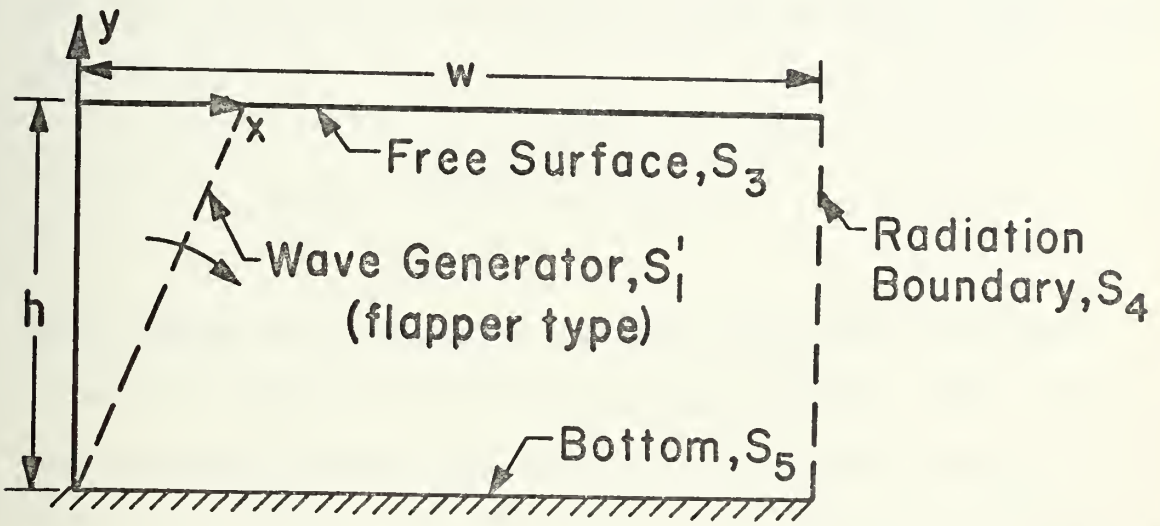

FIGURE 13. Reduced Region for Wave Generator Problem

The boundary condition on S_1' becomes

$$\vec{\nabla}\phi^{(1)}\cdot\vec{n} = q(y) \quad , \quad \text{on } S_1' \quad , \tag{127}$$

The function q(y) describes the mode of displacement of the wave generator. The plunger type and flapper type (shown in figure 13) wave generators were studied and compared with

---

[10] This observation is not true in the potential theory singularity distribution approach. The source singularity must be replaced by doublets and the problem completely reformulated.

MacCamy's results. The function $q_p(y)$ for the plunger type generator is simply

$$q_p(y) = \mu_o \ , \tag{128}$$

where μ_o is the maximum amplitude of the wave generator motion. Similarly, the function $q_f(y)$ for the flapper type generator is

$$q_f(y) = \frac{(h+y)}{h} \mu_o \ . \tag{129}$$

The comparison of MacCamy's results with those obtained herein is shown in figure 14 for the plunger. The circled points were obtained by the FEM and the solid line is MacCamy's theoretical curve. Similarly, the comparison of MacCamy's result for the flapper type wave generator vs the FEM results obtained in this work is shown in figure 15. The excellent agreement allows two observations to be made. First, the FEM approach to solution of problems of the type being presented is highly versatile in its application. Second, the radiation boundary placement was further verified.

D. SECOND-ORDER NUMERICAL RESULTS

1. Semi-Circular Hull – Infinite Depth

The first-order solutions just presented established confidence that second-order solutions could be attempted. The only hull form studied, to the second-order, was semi-circular. The accuracy of the second-order solutions was

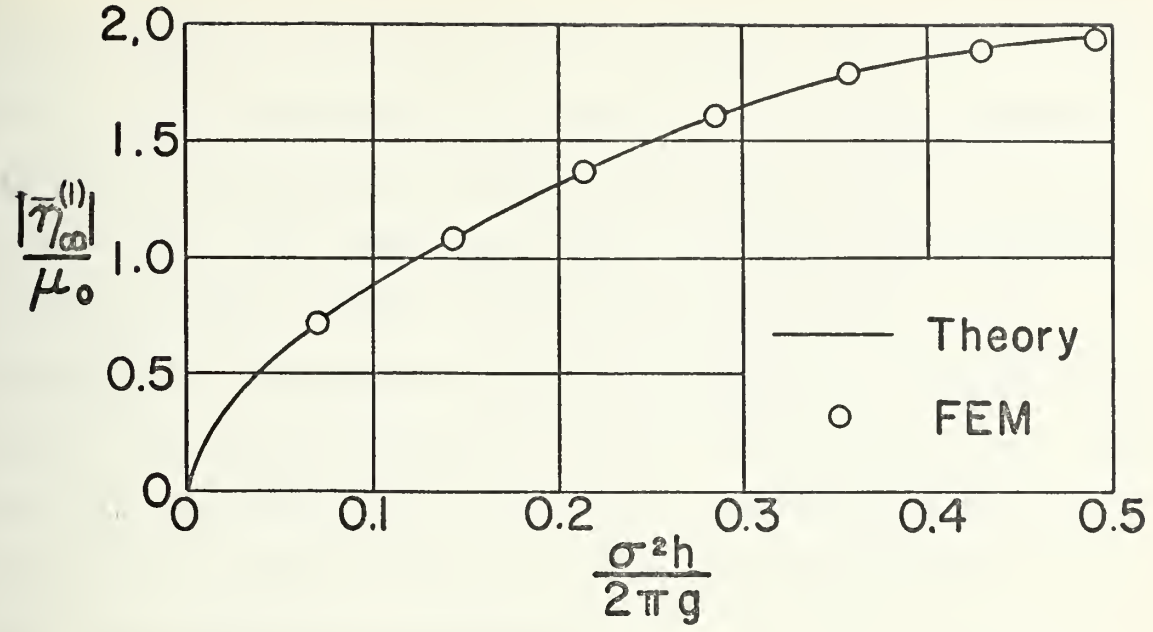

FIGURE 14. Wave Amplitude Generated by a Plunger Type Wave Generator

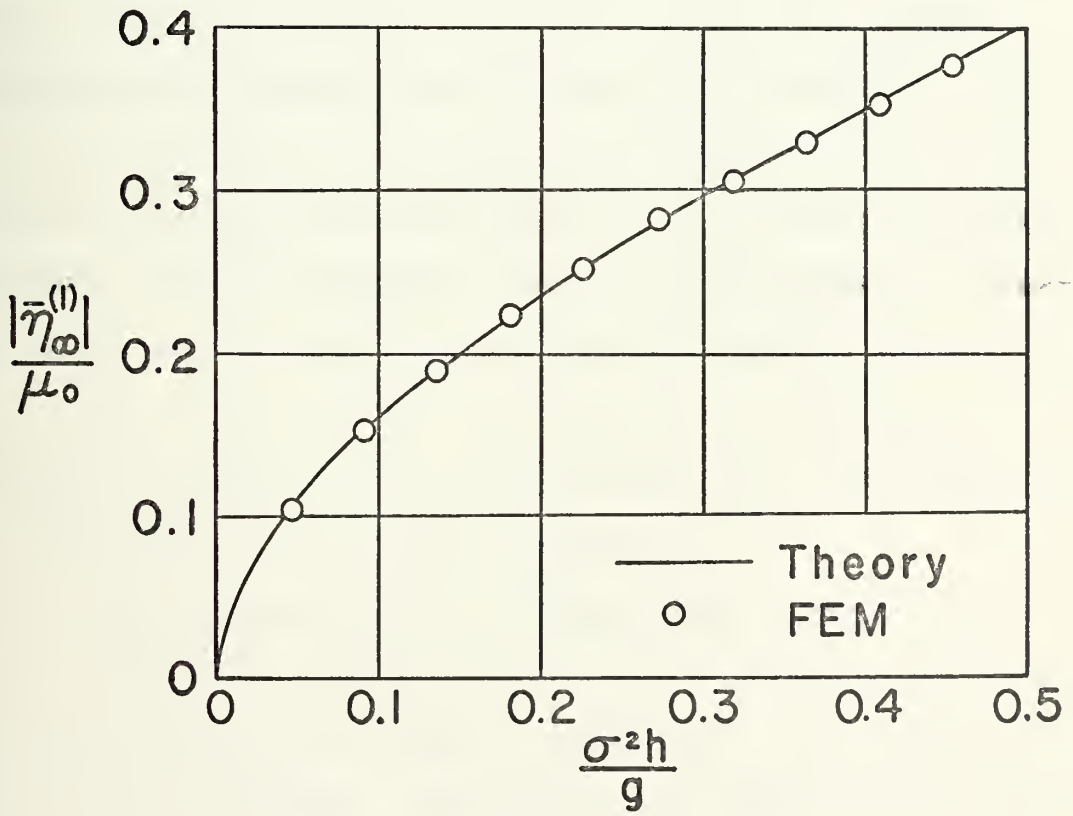

FIGURE 15. Wave Amplitude Generated by a Flapper Type Wave Generator

established by comparing with the work of other researchers. Lee [17,18], Parissis [27], and Potash [31] have reported numerical solutions for second-order exciting force coefficients $\bar{F}_d^{(2)}$, $\bar{F}_s^{(2)}$ and phase angle $\gamma^{(2)}$. Figure 16 compares the values of $\bar{F}_d^{(2)}$ and $\bar{F}_s^{(2)}$ reported by Lee, Parissis, and Potash with the numerical results obtained by the FEM in this work. The points presented from the other researchers' works were all obtained from Potash [31]. Potash indicates Lee's points are corrected in some manner from his original work [17] and otherwise unpublished.

Figure 16 shows excellent agreement for $\bar{F}_s^{(2)}$ and very good agreement for $\bar{F}_d^{(2)}$. Only Potash's points show significant deviation and then only for δ near 1.5. Potash reported some numerical difficulties for a range of δ near 1 and therefore Potash's results are not presented for those values of δ which are suspected to be in error. Similarly, figure 17 shows a comparison of $\gamma^{(2)}$ (phase angle) results. The figure shows the agreement is not as good. However, none of the other works shown (Lee, Parissis, Potash) agree in any consistent fashion over a large range of δ. The reason for the discrepancy has not been resolved.

2. Semi-Circular Hull – Finite Depth

Figure 18 presents the effect of depth on $\bar{F}_d^{(2)}$ and $\bar{F}_s^{(2)}$ as obtained by the FEM in this work. The author knows of no other solutions. Solutions were obtained for values of h/d from 6.0 (infinite depth) to 1.5. The figure shows

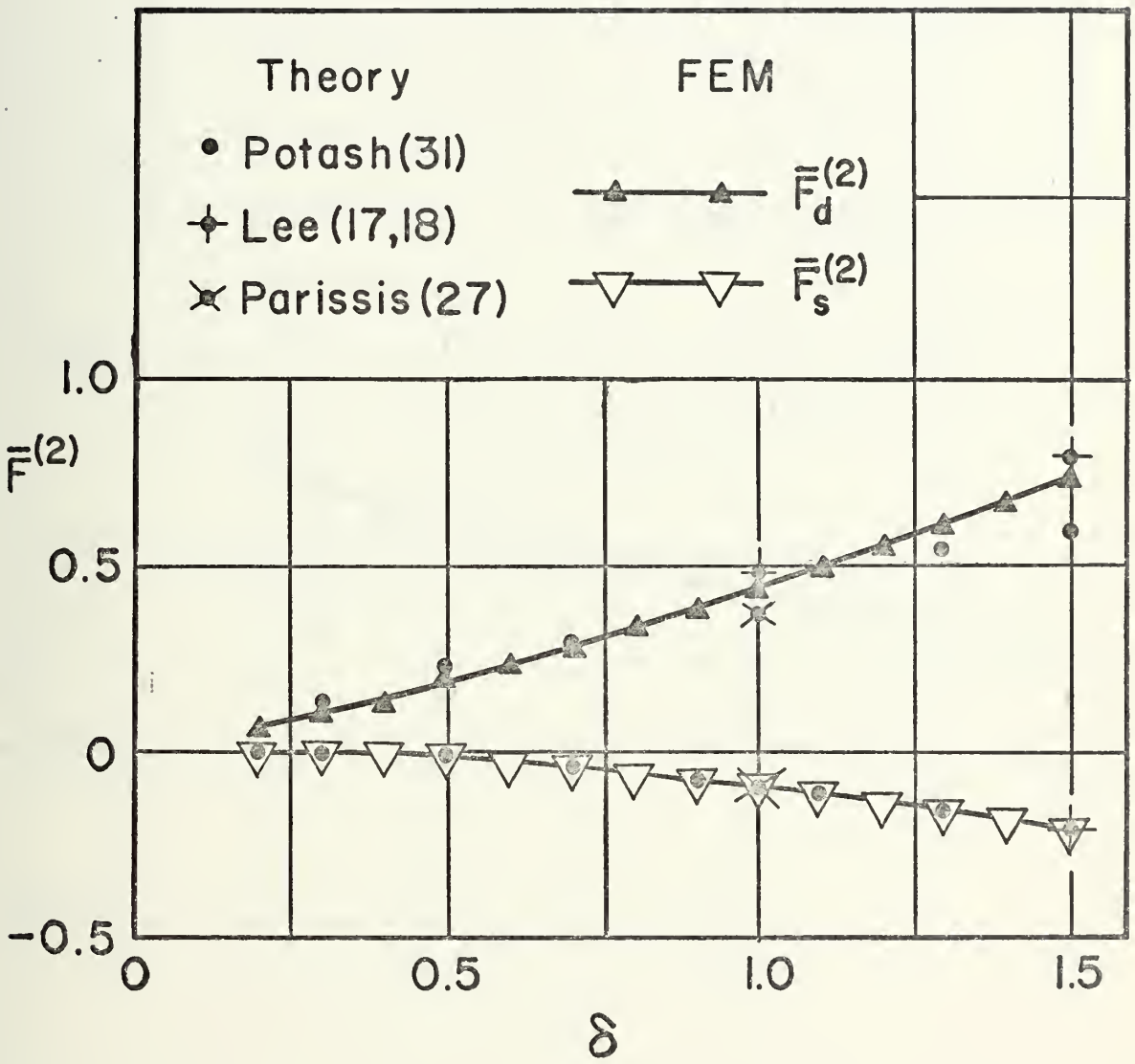

FIGURE 16. Second-Order Exciting Force Amplitude in Heave, Semi-Circular Hull, Infinite Depth

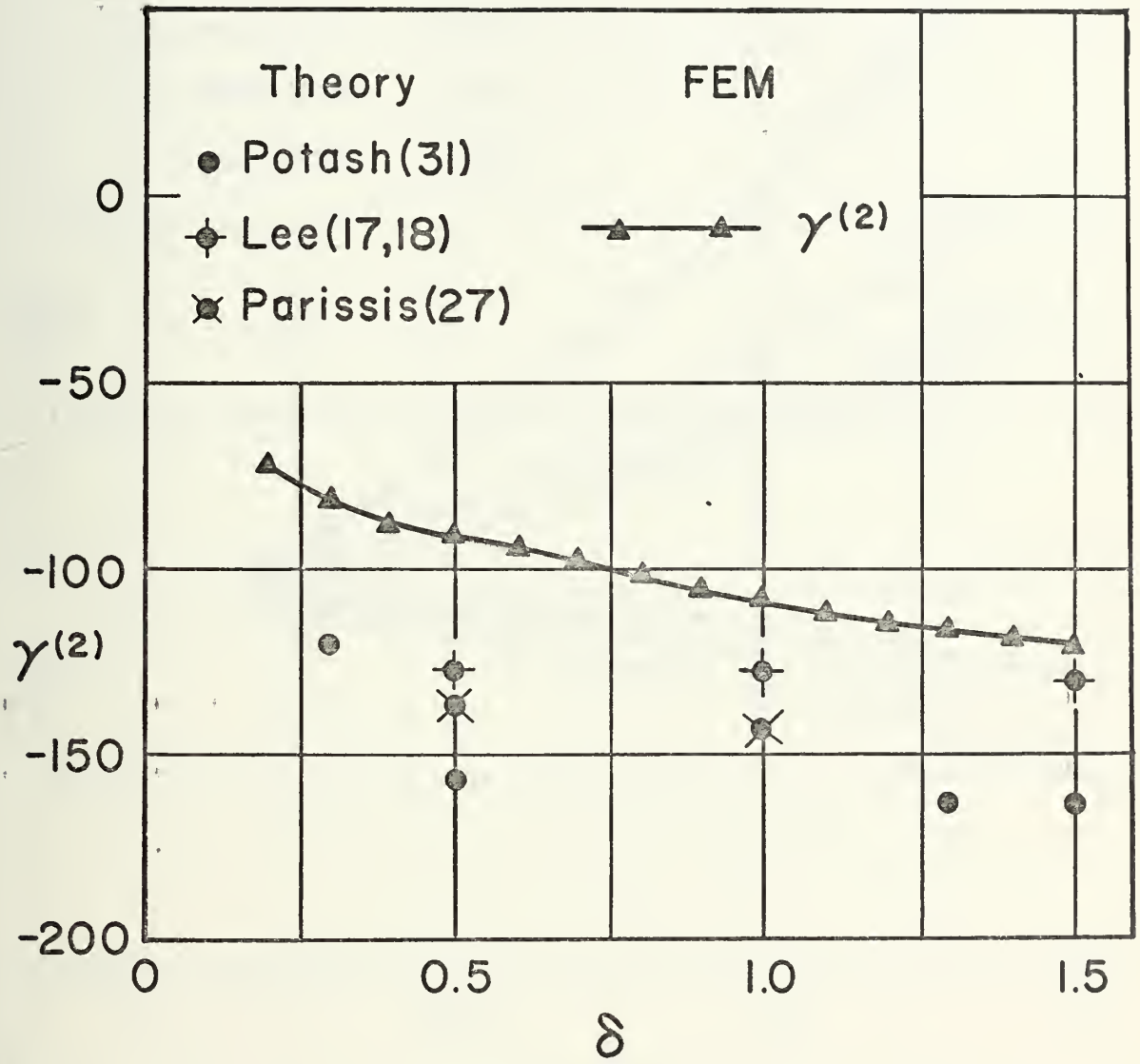

FIGURE 17. Second-Order Exciting Force Phase Angle in Heave, Semi-Circular Hull, Infinite Depth

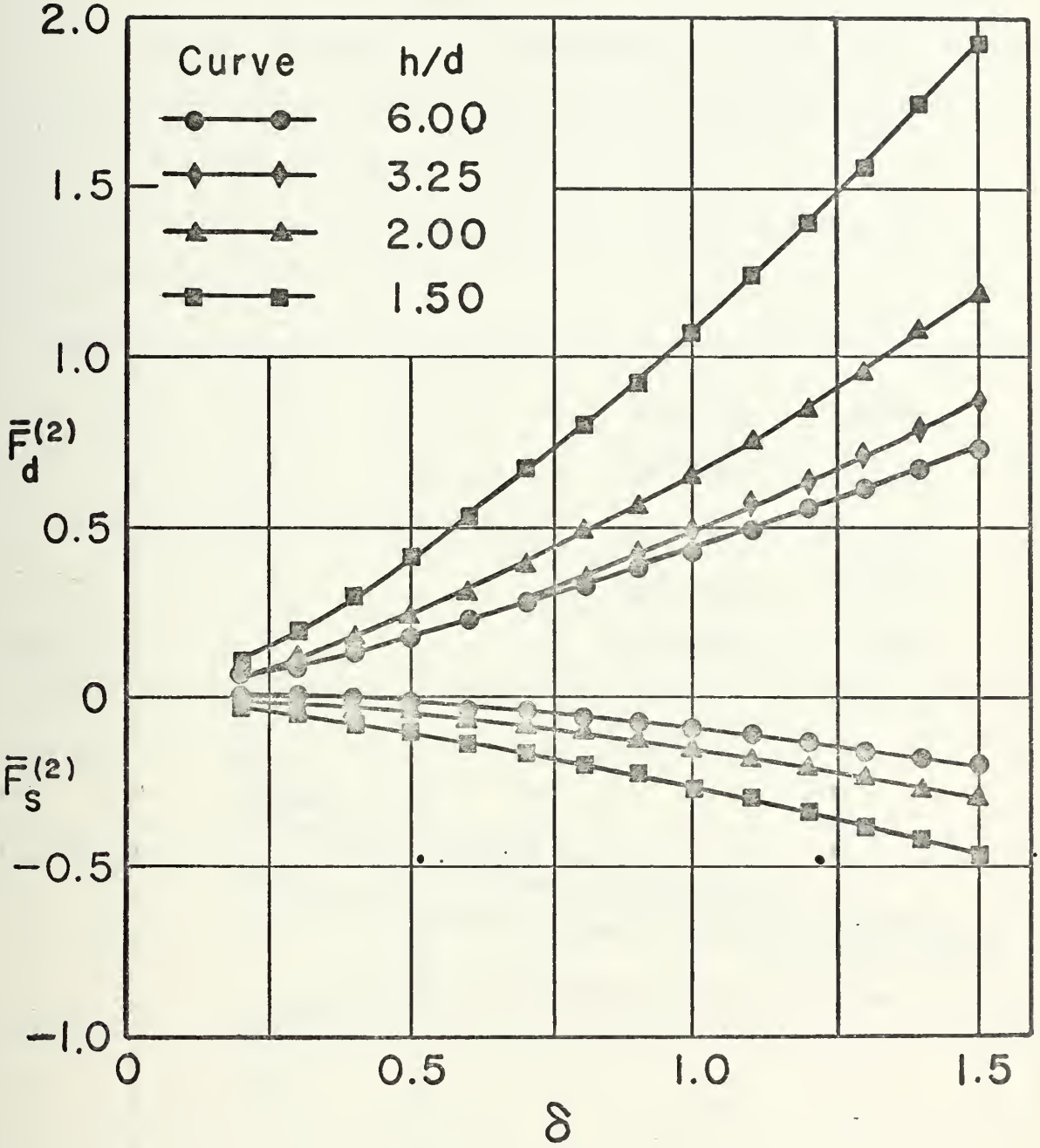

FIGURE 18. Variation of Second-Order Exciting Force Amplitudes with Depth, Semi-Circular Hull in Heave

that $\overline{F}_d^{(2)}$ and $\overline{F}_s^{(2)}$ are most sensitive to finite depth at high values of δ or in very shallow water ($h/d \leq 1.5$).

Figure 19 shows the corresponding effect on $\gamma^{(2)}$ of finite depth for the same range of h/d. Note that at $h/d \cong 1.4$ δ has negligible effect on $\gamma^{(2)}$. Also the effect of decreasing depth causes a monotonic variation of $\gamma^{(2)}$ at fixed δ.

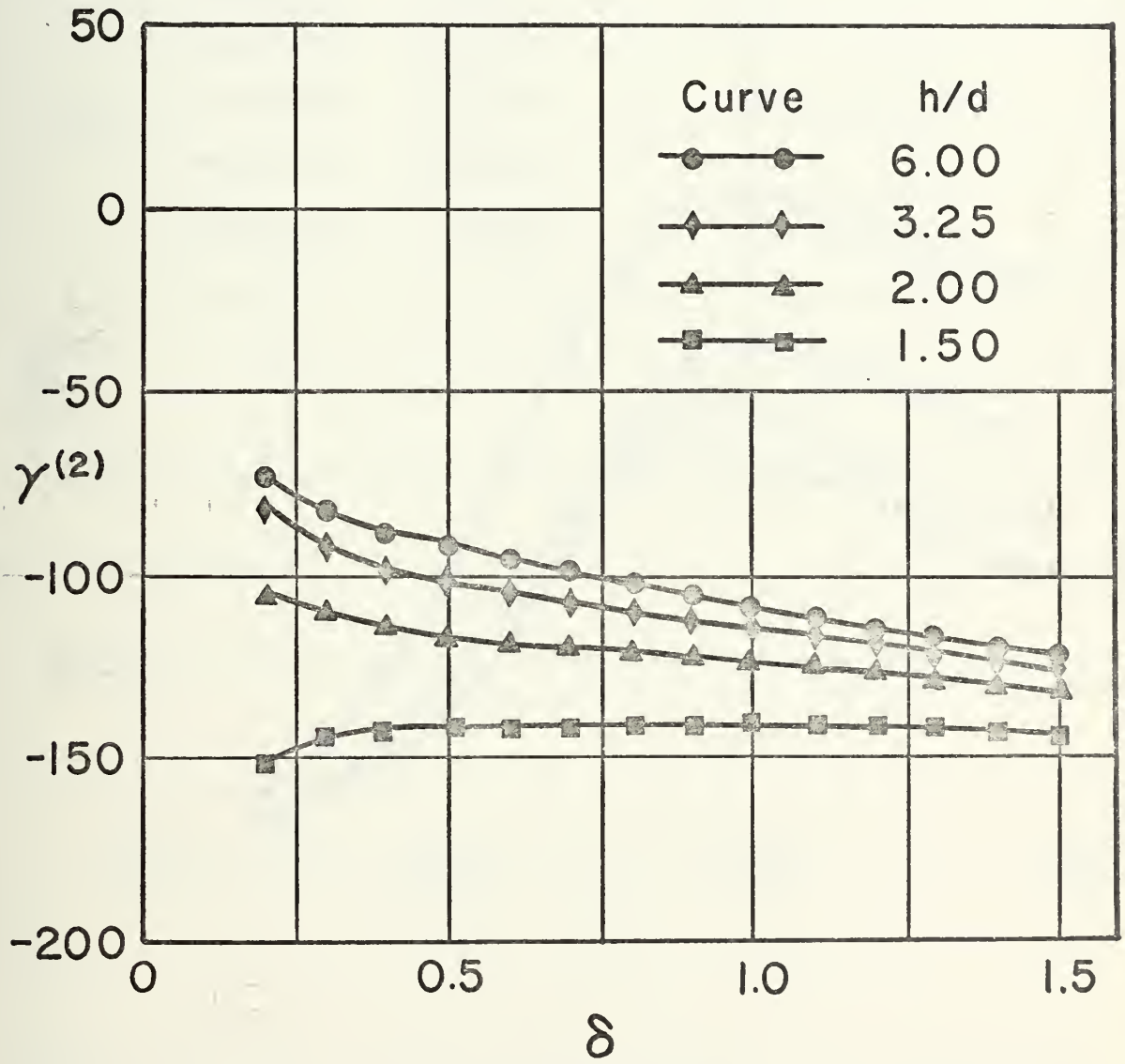

FIGURE 19. Variation of Second-Order Exciting Force Phase Angles with Depth, Semi-Circular Hull in Heave

Figure 20 presents the ratio of $\bar{F}_d^{(2)}$ to $\bar{F}^{(1)}$ plotted vs δ for various values of h/d. The curves peak close to $\delta = 1$ for all values of h/d studied. The curves peak because the first-order force $\bar{F}^{(1)}$ passes through a minimum very near $\delta = 1$ for all values of h/d studied.

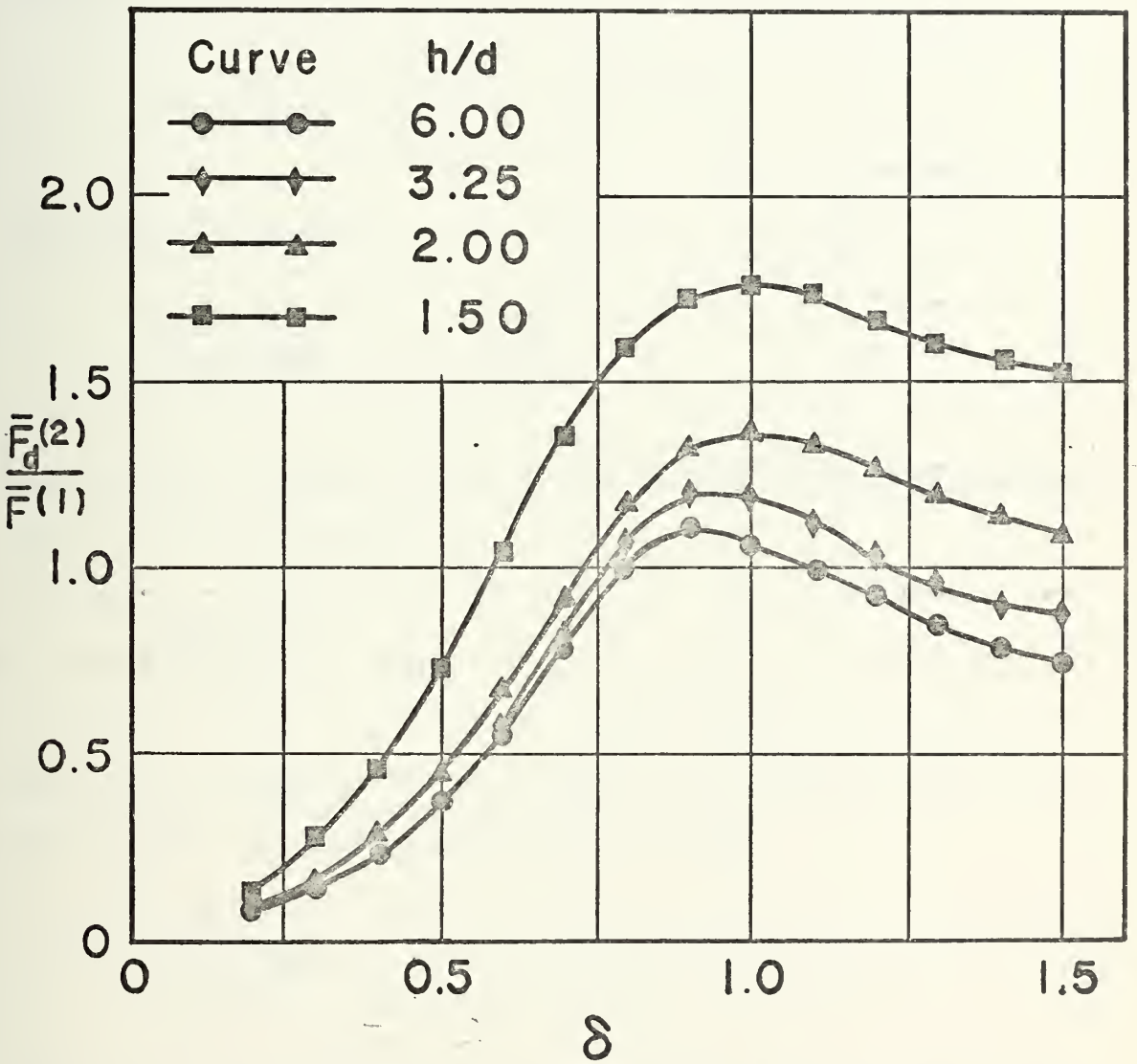

FIGURE 20. Ratio of Second-Order Exciting Force Amplitude to First-Order Exciting Force Amplitude, Semi-Circular Hull in Heave

A quantitative illustration of the physical significance of the nonlinear effects (second-order) is readily made using figure 20. Assume a ship with an approximately circular hull form is being excited such that the maximum acceleration of the motion is 0.2 g's. The maximum time-dependent amplitude of the force is given by

$$|F(t)|_{max} = \varepsilon|f^{(1)}| + \varepsilon^2|f^{(2)}| \quad , \tag{130}$$

which may be written

$$\frac{|F(t)|_{max}}{\varepsilon\ f^{(1)}} = 1 + \varepsilon\ \frac{\bar{F}^{(2)}}{\bar{F}^{(1)}} \quad . \tag{131}$$

Assume h/d = 1.5 and δ = 1.0, the maximum ship acceleration (in g's) may be written

$$\frac{|\ddot{y}(s,t)|}{g} = \varepsilon\ \delta \quad . \tag{132}$$

Equation 132 implies ε = 0.2 under the assumed conditions. Using figure 20 and equations 131 and 132

$$\frac{|F(t)|_{max}}{\varepsilon\ f^{(1)}} = 1 + (0.2)(1.75) = 1.35 \tag{133}$$

Therefore, neglecting the second-order contribution could result in a thirty-five percent error in $|F(t)|_{max}$.

Figure 21 further demonstrates the nonlinear (second-order) effects on F(t). The function $F(t)/\varepsilon\ f^{(1)}$ is plotted

vs t. The ship's displacement as a function of time is also shown on the plot for reference (cosine function of unit amplitude). The parameters chosen for the plot are h/d = 1.5, δ = 1.0 and ε = 0.2 (corresponds to an equivalent acceleration of 0.2 g's).

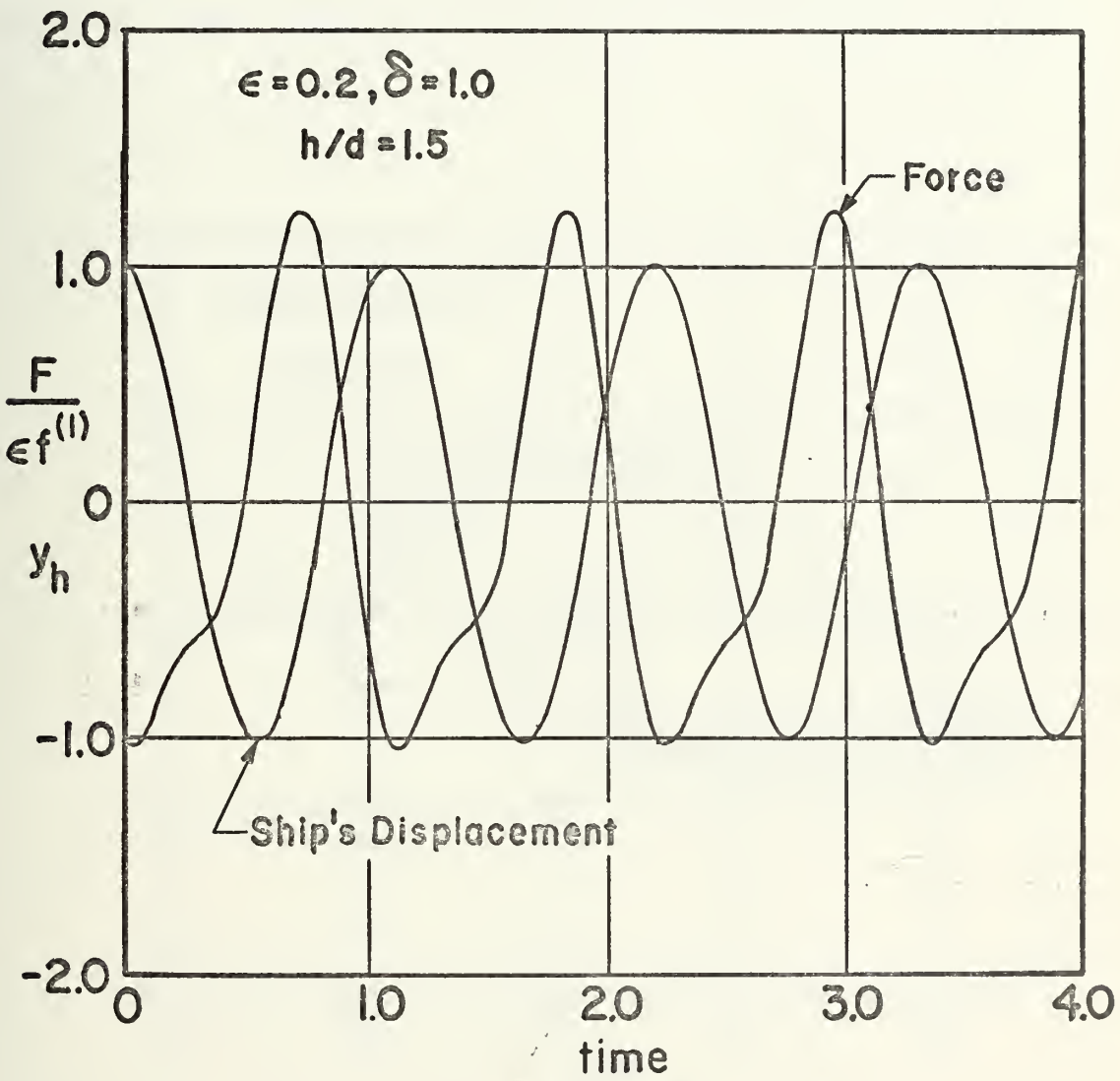

FIGURE 21. Total Exciting Force vs. Time

Figure 22 illustrates, for the same values of the parameters, the nonlinear effects on the gravity wave generated by the ship's disturbance. The figure presents the sum of the dimensionless first-order wave amplitude and the second-order Stokes' wave (both have celerity c_1). Separately, the second-order wave from $\bar{\phi}^{(2)}$ (celerity c_2) is plotted. Both curves are plotted vs x/b for fixed time.

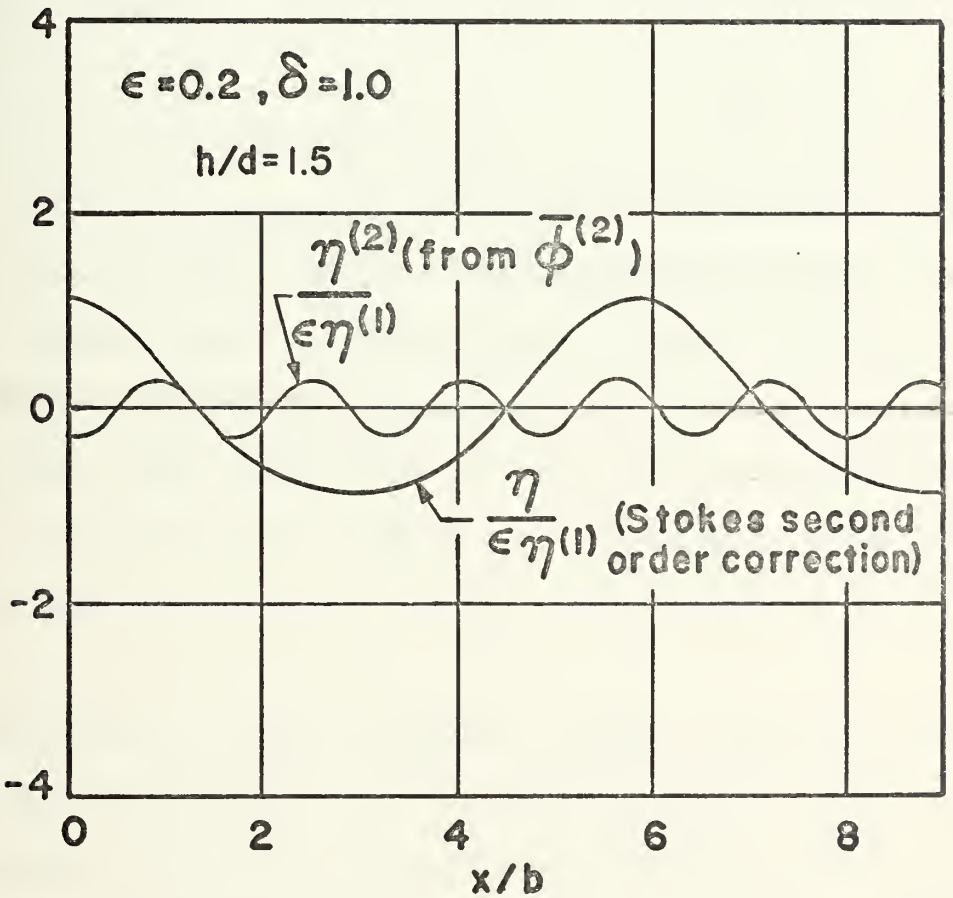

FIGURE 22. Second-Order Wave Form Effects

VI. CONCLUSIONS

It is concluded that this work has demonstrated the feasibility of using the finite element method to solve the linear and nonlinear problems of the type presented. Further, the finite element method is shown to be quite versatile in that various boundary conditions may be applied to the boundary value problems studied, with only minor changes in the computational scheme. In addition, the isoparametric elements chosen are capable of representing arbitrary hull shapes.

It is further concluded that a first-order study of the effect of finite depth on the ship motions studied demonstrates that little change in the solutions occur. However, it is asserted that the second-order results obtained demonstrate that nonlinear (second-order) effects on heaving motions are most significant in very shallow water; particularly for motions at a frequency corresponding very closely to the natural frequency of free oscillations of the floating body.

The present state of digital computer capacity appears to preclude the extension of the present problem to three-dimensions. However, the extension of this study to other modes of motion (sway and roll) is possible as demonstrated for the linear sway problem. Further, the possibility of studying non-symmetric, two-dimensional hull forms is suggested.

An adequate finite element mesh to represent the region for the nonlinear problems studied tends to tax the core capacity of the computer used. Nevertheless, meaningful results were obtained through careful design of the computational scheme.

APPENDIX A

Complex Algebra

The development which follows determines the correct form of the complex numbers w_1 and w_2 in the following expression

$$\mathrm{Re}\{z_1 e^{i\sigma t}\}\mathrm{Re}\{z_2 e^{i\sigma t}\} = \mathrm{Re}\{w_1 + w_2 e^{2i\sigma t}\} \qquad (A1)$$

z_1 and z_2 are complex numbers with moduli r_1 and r_2 and arguments θ_1 and θ_2. It follows using appropriate trigonometric identies that

$$\mathrm{Re}\{r_1 e^{i\theta_1} e^{i\sigma t}\}\mathrm{Re}\{r_2 e^{i\theta_2} e^{i\sigma t}\} =$$

$$r_1 r_2[\cos\theta_1\cos\theta_2\ \tfrac{1}{2}(1+\cos 2\sigma t) + \sin\theta_1\sin\theta_2\ \tfrac{1}{2}(1-\cos 2\sigma t)$$

$$-\sin(\theta_1+\theta_2)\tfrac{1}{2}\sin 2\sigma t] = \frac{r_1 r_2}{2}\,[\cos(\theta_1-\theta_2) + \cos(\theta_1+\theta_2+2\sigma t)] \qquad (A2)$$

Equation A2 implies that

$$w_1 = \frac{z_1\tilde{z}_2}{2} \quad , \quad w_2 = \frac{z_1 z_2}{2} \quad . \qquad (A3)$$

The symbol ($\tilde{}$) implies conjugation.

Equation A3 shows the origin of the factor ½ in various places in the text.

APPENDIX B

Isoparametric Elements

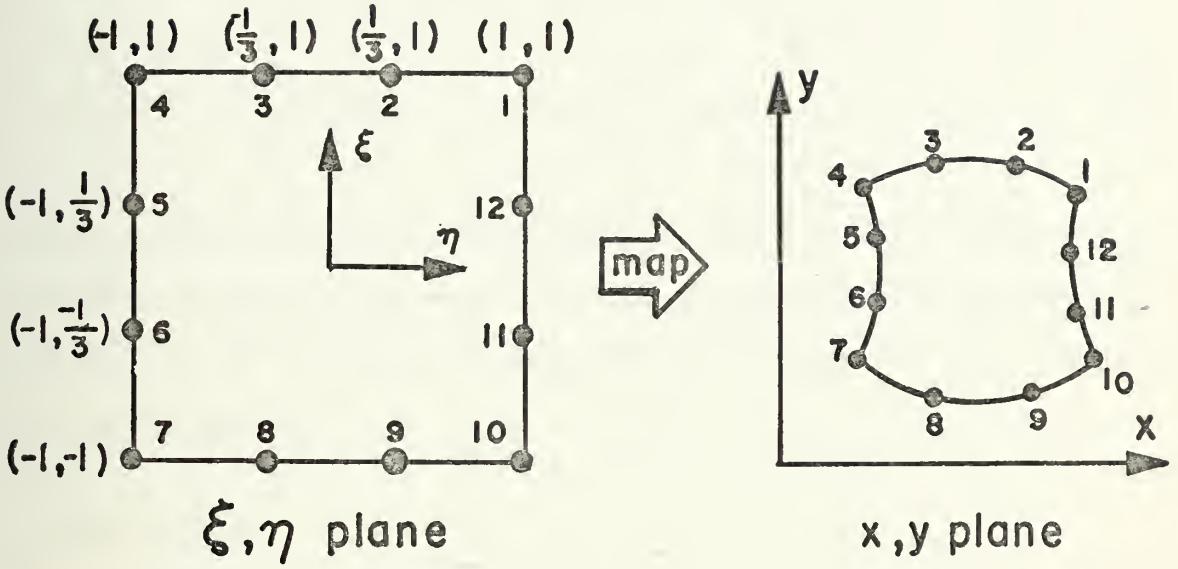

FIGURE B1. Element Mapping from ξ,η Plane to x,y Plane

The essential idea in the isoparametric element lies in the following equations which define a map from the ξ,η plane to the x,y plane.

$$x = \underset{\sim}{N}^e \underset{\sim}{x}^e \quad , \tag{B1}$$

$$y = \underset{\sim}{N}^e \underset{\sim}{y}^e \tag{B2}$$

The vector $\underset{\sim}{N}^e$ is a 1 x 12 row vector of element shape functions one for each node in figure B1. The vectors $\underset{\sim}{x}^e$ and $\underset{\sim}{y}^e$ are

12 x 1 column vectors representing the respective x and y coordinates of the nodes in the x,y plane (figure B1).

The shape functions are conveniently defined using the conventions of Zienkiewicz [45]. Let

$$\xi_o = \xi\xi_i \quad , \quad \eta_o = \eta\eta_i \quad , \tag{B3}$$

where ξ and η are the coordinates of any point of the square element in the ξ,η plane. ξ_i and η_i are the coordinates of the i^{th} node. The shape functions are given by the following set of equations.

Corner Nodes:

$$N_i^e = \frac{1}{32}(1 + \xi_o)(1 + \eta_o)[-10 + 9(\xi^2 + \eta^2)] \ , \tag{B4}$$

Edge Nodes:

$$\text{for } \xi_i = \pm 1, \quad \eta_i = \pm\frac{1}{3} \ ,$$

$$N_i^e = \frac{9}{32}(1 + \xi_o)(1 - \eta^2)(1 + 9\eta_o) \ , \tag{B5}$$

$$\text{for } \xi_i = \pm\frac{1}{3} \ , \quad \eta_i = \pm 1 \ ,$$

$$N_i^e = \frac{9}{32}(1 + \eta_o)(1 - \xi^2)(1 + 9\xi_o) \tag{B6}$$

The element is defined to be isoparametric when the same shape functions are used to achieve the element mapping as are used to define the field function in the x,y plane. There are certain consistency requirements on the element shape functions as discussed by Zienkiewicz [45]. The shape functions chosen satisfy them all.

The mapping has the advantage of being able to represent a region with curvilinear sides. The area and line integrals given in part III are calculated by the expressions given below.

From the calculus, the following relation is known to hold

$$\begin{bmatrix} N^e_{\sim\xi} \\ N^e_{\sim\eta} \end{bmatrix} = \underset{\approx}{J} \begin{bmatrix} N^e_{\sim x} \\ N^e_{\sim y} \end{bmatrix} \tag{B7}$$

$\underset{\approx}{J}$ is the real 2 x 2 Jacobian matrix of the transformation.

$$\underset{\approx}{J} = \begin{bmatrix} N^e_{\sim\xi} x^e & N^e_{\sim\xi} y^e \\ N^e_{\sim\eta} x^e & N^e_{\sim\eta} y^e \end{bmatrix} \tag{B8}$$

It follows, provided $\underset{\approx}{J}$ is not singular, that

$$\begin{bmatrix} N^e_{\sim x} \\ N^e_{\sim y} \end{bmatrix} = \underset{\approx}{J}^{-1} \begin{bmatrix} N^e_{\sim\xi} \\ N^e_{\sim\eta} \end{bmatrix} \tag{B9}$$

Then, for example, equation 86 in part III may be written at the element level as

$$\underset{\approx}{H}^e = \int_{Re} \begin{bmatrix} \underset{\sim}{N}_x^{eT} & \underset{\sim}{N}_y^{eT} \end{bmatrix} \begin{bmatrix} \underset{\sim}{N}_x^e \\ \\ \underset{\sim}{N}_y^e \end{bmatrix} dRe \qquad \text{(B10)}$$

Using equations B8, B9, and

$$dRe = dxdy = |\underset{\approx}{J}| \, d\xi d\eta \quad , \qquad \text{(B11)}$$

equation B9 may be written

$$\underset{\approx}{H}^e = \int_{-1}^{+1} \int_{-1}^{+1} \begin{bmatrix} \underset{\sim}{N}_\xi^{eT} & \underset{\sim}{N}_\eta^{eT} \end{bmatrix} [\underset{\approx}{J}^{-1}]^T [\underset{\approx}{J}^{-1}] \begin{bmatrix} \underset{\sim}{N}_\xi^e \\ \\ \underset{\sim}{N}_\eta^e \end{bmatrix} |\underset{\approx}{J}| \, d\xi d\eta \; . \qquad \text{(B12)}$$

Equation B12 demonstrates the method of the evaluation of the matrix $\underset{\approx}{H}^e$ or in general the matrix $\underset{\approx}{H}$. The integrations are accomplished using six-point Gauss quadrature.

APPENDIX C

Computer Program Economization

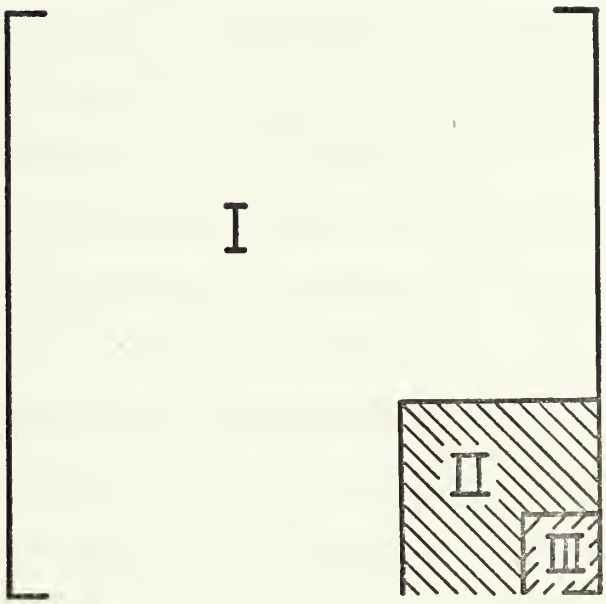

FIGURE C1. Schematic of Coefficient Matrix

The economizations in the computer solution of the linear system of equations defined by equation 102 in part IV are achieved by observing certain properties of the matrix $\underset{\approx}{K}^{(1)}$. First all interior nodes of a given mesh contribute only real numbers to $\underset{\approx}{K}^{(1)}$. This is also true of nodes on S_1, S_2 and S_3. Only the nodes on S_4 contribute complex entries in $\underset{\approx}{K}^{(1)}$. Further only nodes on S_3 and S_4 contribute entries which are frequency dependent.

The nodes on S_3 and S_4 typically comprise no more than fifteen percent of $\underset{\approx}{K}^{(1)}$. Further, the nodes on S_4 alone

comprise nor more than five percent of the total rows in $\underset{\approx}{K}^{(1)}$. Therefore if $\underset{\approx}{K}^{(1)}$ is rearranged with equations for nodes on S_4 at the bottom, equations for S_3 nodes directly above the S_4 equations, and all other rows of the matrix filling the remaining part of $\underset{\approx}{K}^{(1)}$, the resulting matrix would appear as schematically represented in figure C1. The region designated with a Roman numeral I (uncrosshatched) indicates the portion of the matrix completely real and frequency independent.

Region II indicates the portion of the matrix which has elements that are frequency dependent. And, Region III indicates the portion of the matrix which is complex and frequency dependent. If the matrix $\underset{\approx}{K}^{(1)}$ is formed as shown in figure C1, eighty-five percent (approximately) of it may be eliminated only once using real arithmetic. This is possible because the matrix $-\sigma^2\underset{\approx}{Q}_0$ does not have to be added to Region II until after Region I has been reduced by Gauss elimination, and the same fact applies to the matrix $(i\sigma/c_1)\underset{\approx}{D}$ in Region III. Then, after Region I is eliminated, the matrix $-\sigma^2\underset{\approx}{Q}_0$ is added to Region II (after saving the previous results) and $\underset{\approx}{K}^{(1)}$ is reduced to upper triangular form through Region II using real arithmetic. Now, if this result is saved and then the matrix $(i\sigma/c_1)\underset{\approx}{D}$ is added to Region III only a small set of complex equations (usually about 25) is left to solve.

After the final elimination, the resulting matrix is in complete upper-triangular form and ready for a back-substitution process. The right-hand side vector is complex

and frequency dependent in general. However, the required information to perform the forward substitution process on it is contained in the final form of $\underset{\approx}{K}^{(1)}$ (upper triangular). Therefore, the forward substitution on $ibo\underset{\sim}{r}^{(1)}$ may be done after $\underset{\approx}{K}^{(1)}$ is processed. Then a back-substitution of the resulting system using mixed-mode computer arithmetic yields the final solution vector $\underset{\sim}{\phi}^{(1)}$.

A close examination of the process just described reveals that for a whole family of frequencies only a small portion of $\underset{\approx}{K}^{(1)}$ has to be reassembled and eliminated again. These matrix properties contribute toward a sizeable saving in computer time.

BIBLIOGRAPHY

1. Adamek, J. R., An Automatic Mesh Generator Using Two and Three-Dimensional Isoparametric Elements, M. S. Thesis, Naval Postgraduate School, Monterey, California, 1973.

2. Allouard, Y., and Coubert, J.F., "Numerical Study of Transitory or Non-Linear Waves," Proceedings of the International Symposium on Finite Element Methods in Flow Problems, Swansea, January, 1974, pp. 283-288.

3. Bai, K. J., "A Variational Method in Potential Flows with a Free Surface," University of California, Berkeley, College of Engineering, Report No. NA 72-2, 1972.

4. Chenault, D. W., II, Motion of a Ship at the Free Surface, M. S. Thesis, Naval Postgraduate School, Monterey, California, 1970.

5. Fontannet, P., "Theorie de la Generation de la Houle Cylindrique par un Batteur Plan (2^e Order d'Approximation)," La Houille Blanche, Vol. 16, 1961, pp. 179-197.

6. Frank, W., "Oscillations of Cylinders in or Below the Free Surface," Naval Ship Research and Development Center, Report No. 2375, October, 1967, pp. 1-48.

7. Garrison, C. J., The Consistent Second-Order Theory of Wave/Structure Interaction, paper to be presented at the 14th International Conference on Coastal Engineering, Copenhagen, 24-28 June, 1974; To be published in the Proceedings of the above: September, 1974.

8. Garrison, C. J., "Hydrodynamics of Large Objects in the Sea Part I - Hydrodynamic Analysis," Journal of Hydronautics, Vol. 8, No. 2, January, 1974, pp. 5-12.

9. Grim, O., "Berechnung der durch Schwingungen Eines Schiffskorpers Erzeugten Hydrodynamischen Krafte," der Schiffbautech. Ges., Vol. 47, 1953, pp. 277-296.

10. Havelock, T., Philosophical Magazine, Vol. 8, No. 51, October 1929, pp. 569-576.

11. Havelock, T., "Waves Due to a Floating Sphere Making Periodic Heaving Oscillations," Proceedings Royal Society of London, Vol. 231, 1955, pp. 1-7.

12. Holand, I., "Finite Elements for the Computation of Hydrodynamic Mass," Proceedings of the Symposium on Finite Element Techniques, Stuttgart, 1969, pp. 509-531.

13. John, F., "On the Motion of Floating Bodies," Communications on Pure and Applied Mathematics, Vol. 3, 1950, pp. 45-101.

14. Kim, C. H., "Hydrodynamic Forces and Moments for Heaving, Swaying, and Rolling Cylinders on Water of Finite Depth," Journal of Ship Research, Vol. 13, No. 2, 1969, pp. 137-154.

15. Lamb, H., Hydrodynamics, Cambridge University Press, 6th edition, 1932.

16. Landweber, L., and Macagno, M., "Added Mass of a Three Parameter Family of Two Dimensional Forms," Journal of Ship Research, Vol. 2 , No. 4, 1959, pp. 36-48.

17. Lee, C. M., "The Second-Order Theory of Cylinders Oscillating in a Free Surface," University of California, Berkeley, College of Engineering, Report No. NA-66-7, September, 1966.

18. Lee, C. M., "The Second-Order Theory of Heaving Cylinders in a Free Surface," Journal of Ship Research, Vol. 12, 1968, pp. 313-327.

19. Lewis, F. M., "The Inertia of Water Surrounding a Vibrating Ship," Transactions of the Society of Naval Architects and Marine Engineers, Vol. 37, 1929, pp. 1-20.

20. MacCamy, R. C., "A Source Solution for Short-Crested Waves," La Houille Blanche, No. 3, July-August, 1957, pp. 373, 379-389.

21. Matsumoto, K., "Application of Finite Element Method to Added Virtual Mass of Ship Hull Vibration," Journal of the Society of Naval Architects of Japan, Vol. 127. 1970, pp. 83-90.

22. Matsuura, Y., and Kawakami, M., "Calculation of Added Virtual Mass Moment of Inertia of Ship Hull Vibration by the Finite Element Method," Journal of the Society of Naval Architects of Japan, Vol. 124, 1968, pp. 281-291.

23. Newton, R. E., Chenault, D. W., II, and Smith, D. A., Jr., "Finite Element Solution for Added Mass and Damping," Proceedings of the International Symposium on Finite Element Methods in Flow Problems, Swansea, January, 1974, pp. 159-170.

24. Newton, R. E., Finite Element Analysis of Two-Dimensional Added Mass and Damping, to be published in Collection of Papers presented at the International Symposium on Finite Element Methods in Flow Problems, Swansea, J. Wiley and Sons, London.

25. Ogilvie, T. F., "First and Second-Order Forces on a Cylinder Submerged Under a Free Surface," Journal of Fluid Mechanics, Vol. 16, 1963, pp. 451-472.

26. Ogilvie, T. F., and Tuck, E. O., "A Rational Strip Theory of Ship Motions," University of Michigan, Department of Naval Architecture, Report No. 013, 1969.

27. Parissis, G., "Second-Order Potentials and Forces for Oscillating Cylinders on a Free Surface," Massachusetts Institute of Technology, Report No. 66-10, 1966.

28. Paulling, J. R., and Richardson, R., "Measurement of Pressures, Forces, and Radiating Waves for Cylinders Oscillating in a Free Surface," University of California, Berkeley, Report No. 82-28, 1962.

29. Paulling, J. R., and Porter, W. R., "Analysis and Measurement of Pressure and Force on Heaving Cylinders in a Free Surface," Proceedings of the Fourth National Congress of Applied Mechanics, 1962, pp. 1369-1382.

30. Porter, W. R., "Pressure Distributions, Added-Mass, and Damping Coefficients for Cylinders Oscillating in a Free Surface," University of California, Berkeley, Report No. 82-16, 1960.

31. Potash, R. L., "Second-Order Theory of Oscillating Cylinders," University of California, Berkeley, Report No. NA70-3, 1970.

32. Roren, E. M. Q., "Impact of Finite Element Techniques on Practical Design of Ships Structures," Proceedings of the Symposium on Finite Element Techniques, Stuttgardt, 1969, pp. 509-531.

33. Salveson, N., On Second-Order Wave Theory for Submerged Two-Dimensional Bodies, Ph. D. Dissertation, University of Michigan, Ann Arbor, 1966.

34. Saunders, H. E., Hydrodynamics in Ship Design, Vol. 2, The Society of Naval Architects and Marine Engineers, New York, 1957.

35. Stoker, J. J., Water Waves, Interscience Publishers, Inc., New York, 1957, pp. 19-54.

36. Tasai, F., "Damping Forces and Added Mass of Ships Heaving and Pitching," Kyushu University, Research Institute of Applied Mechanics, Report, Vol. 8, pp. 131-152, 1959; Vol. 8, pp. 36-39, 1960.

37. Tuck, E. O., "The Effect of Non-Linearity at the Free Surface on Flow Past a Submerged Cylinder," Journal of Fluid Mechanics, Vol. 22, 1965, pp. 401-414.

38. Ursell, F., "On the Heaving Motion of a Circular Cylinder on the Surface of a Fluid," Quarterly Journal of Applied Mechanics and Applied Mathematics, Vol. 2, No. 2, 1949, pp. 218-231.

39. Visser, W., and van der Wilt, M., "A Numerical Approach to the Study of Irregular Ship Motions," Proceedings of the International Symposium on Finite Element Methods in Flow Problems, Swansea, January, 1974, pp. 277-282.

40. Vugts, J., "The Hydrodynamic Coefficients for Swaying, Heaving, and Rolling Cylinders in a Free Surface," Netherlands Ship Research Center, Report No. 1125, 1968.

41. Wehausen , J.V. , and Laitone, E. V., Surface Waves Encyclopedia of Physics, Vol. 9, edited by S. Flugge, Springer-Verlag, Berlin, 1960.

42. Yu, Y.S., and Ursell, F., "Surface Waves Generated by an Oscillating Cylinder on Water of Finite Depth: Theory and Experiment," Journal of Fluid Mechanics, Vol. 11, No. 4, 1961, pp. 529-551.

43. Zienkiewicz, O. C., and Newton, R. E., "Coupled Vibrations of a Structure Submerged in a Compressible Fluid," Proceedings of the Symposium on Finite Element Techniques, Stuttgart, 1969, pp. 359-379.

44. Zienkiewicz, O. C., Irons, B. M., and Nath, B., "Natural Frequencies of Complex Free or Submerged Structures by the Finite Element Method," Proceedings of the Conference on Vibrations in Civil Engineering, Institution of Civil Engineers, London, 1965.

45. Zienkiewicz, O. C., The Finite Element Method in Engineering Science, McGraw-Hill, London, 1971.

46. Zienkiewicz, O. C., and Cheung, Y. K., "Finite Elements in the Solution of Field Problems," The Engineer, September, 1965, pp. 507-510.

INITIAL DISTRIBUTION LIST

		No. Copies
1.	Defense Documentation Center Cameron Station Alexandria, Virginia 22314	2
2.	Library, Code 0212 Naval Postgraduate School Monterey, California 93940	2
3.	Professor R. E. Newton, Code 59Ne Department of Mechanical Engineering Naval Postgraduate School Monterey, California 93940	2
4.	Commander, Naval Shipyard. Att: LT David A. Smith, Jr., Code 338.22 Long Beach, California 91701	1
5.	Professor J. R. Paulling Department of Naval Architecture University of California Berkeley, California 94720	1
6.	Naval Ship Research and Development Center Engineering Research Project in Hydromechanics Bethesda, Maryland 20034	1
7.	Naval Ship Systems Command Headquarters Code 03 Navy Department Washington, D. C. 20360	1

150953

Thesis
S5759 Smith
c.1 Finite element analysis of the forced oscillations of ship hull forms.